3 Results

3.1 Characterisation of the Bboxes of MID1

As previously described, most of the so far characterised OS patients harbour mutations in the C-terminal domain of MID1, that disrupt the association with microtubules and result in aggregation of the mutant protein in cytosolic clumps. In contrast, these mutations do not affect the interaction with α4, regulatory subunit of PP2A, which is then recruited to the cytoplasmic clumps, leading to accumulation of microtubule-associated PP2Ac (introduction section 1.2.2). Except for microtubule-association of the C-terminus and α4-binding properties of the Bbox1 domain of MID1, functions of other MID1 regions (including Bbox2) are largely unknown.

Knowing that MID1 interacts with α4 through the Bbox1 domain (Trockenbacher et al., 2001), and assuming that Bbox2 might participate in the regulation of the MID1 protein function (Winter et al., 2004), a series of experiments was performed in order to elucidate and characterise the function of the two Bboxes of MID1.

3.1.1 Mutations in Bbox1 disrupt MID1-α4 interaction

Mutation analysis on DNA from OS patients is being performed on a regular basis in our laboratory. Recently, two new mutations located in exon1 of MID1 were identified in two unrelated patients. One patient was found to have a 388G>A mutation, predicting a change of an alanine into a threonine at position 130 (A130T) in the Bbox1 domain of MID1. The second patient had a 433T>A mutation, predicting a cysteine to serine change at position 145 (C145S) also located in Bbox1. Both were *de novo* mutations.

To date, only two mutations in the Bboxes of MID1 have been described in the literature, namely deletion of a valine, theronine and cysteine at positions 135 to 138 (ΔVTC) in Bbox1 (De Falco et al., 2003; Pinson et al., 2004) and an amino acid change of a cysteine into a phenylalanine at position 195 (C195F) in Bbox2 (De Falco et al., 2003), both resulting in severe OS phenotypes. The novel mutations described in this thesis were also identified in severely affected individuals, supporting an important role of the Bboxes for the correct functioning of MID1. Since MID1 interacts with α4 through its Bbox1 domain, it was first tested whether mutations in this domain lead to disruption of the MID1-α4 interaction.

The following N-terminally green fluorescent protein (GFP)-tagged MID1 constructs carrying different mutations in the Bbox1 domain were used in this study:

- **A130T, C145S**: novel identified mutations in OS patients in our laboratory.
- **ΔVTC:** published mutation in Bbox1 (above described).
- **ΔBbox1**: deletion of the entire Bbox1 domain.

These constructs, as well as wild-type MID1, were co-expressed in COS-7 cells together with V5-tagged α4, and their subcellular localisation was examined by immunostaining. While MID1 constructs were followed by the presence of the GFP-tag, anti-V5 and subsequent anti-mouse Cy3 labelled antibodies were used to assess α4 localisation (subsequent experiments were done in the same manner). As previously reported (Trockenbacher et al., 2001), α4 alone localised diffusely in the cytosol (Figure 3.1A) and in the presence of wild-type MID1, it was tethered to the microtubules (Figure 3.1B-wild-type). As expected, in contrast to the wild-type form (Figure 3.1B, wild-type), Bbox1 mutated or deleterious MID1 forms were unable to bind α4 *in vivo* (Figure 3.1B, ΔBbox1, 130T, C145S and ΔVTC). While point mutated MID1 could still bind to microtubules, α4 remained spread all over the cell. Of note, deletion of the entire Bbox1 also seemed to slightly influence microtubule binding-properties of the protein.

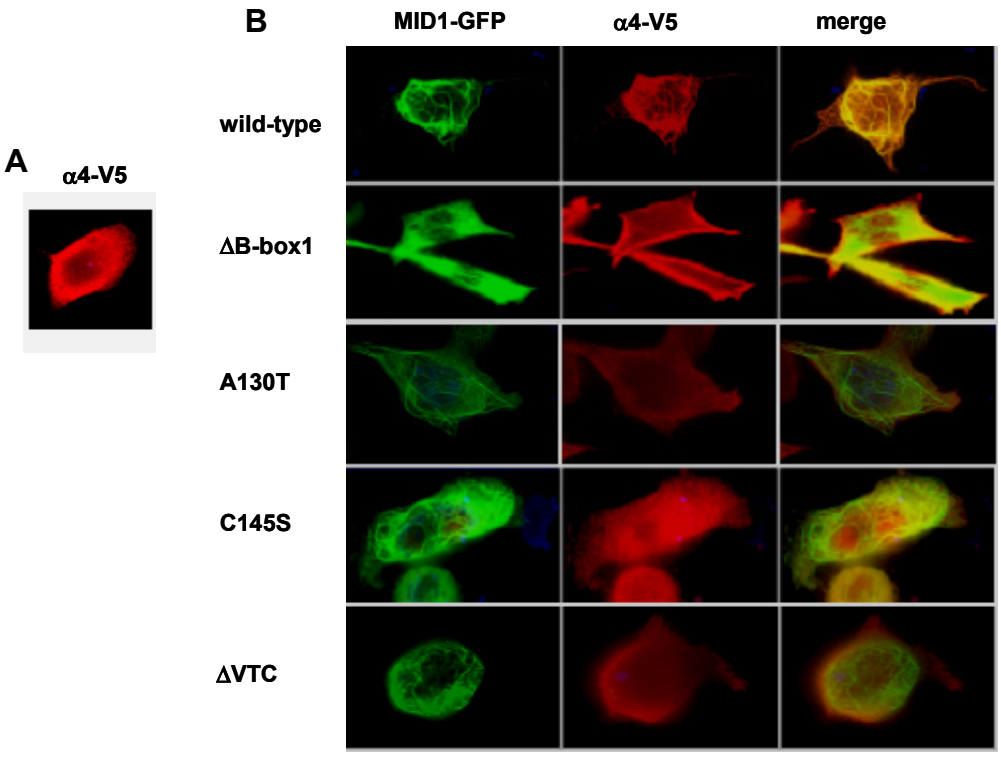

Figure 3.1. Bbox1 mutated MID1 and α4 localisation

A. Cytosolic localisation of α4-V5 overexpressed in COS-7 cells, stained with anti-V5 and subsequent anti-mouse Cy3 labelled antibody. **B**. COS-7 cells co-expressing different MID1 constructs (wild-type, deletion of Bbox1, A130T and C145S mutations and deletion of VTC (ΔVTC)) and α4 were immunostained. GFP shows MID1 localisation in green and α4-V5 is stained in red with Cy3. The merge image of both signals is shown to the right.

For further verification, co-immunoprecipitation experiments were performed in COS-7 cells co-expressing different N-terminally FLAG-tagged MID1 (MID1-FLAG) constructs (A130T, ΔBbox1 and wild-type) and N-terminally myc-tagged α4 (α4-myc) (Figure 3.2A). Immunoprecipitation experiments were performed with anti-FLAG and anti-myc antibodies (Figures 3.2B and 3.2C respectively) and Western blots of the precipitates were developed with the corresponding antibodies, anti-myc or anti-FLAG respectively. Cells expressing α4-myc alone were used as background control. Co-precipitation of α4 and MID1 could only be shown with wild-type MID1 but not with either of the mutant proteins (Figure 3.2B-lower lane and 3.2C-upper lane), independently of the antibody used for the immunoprecipitation. Both blots were also incubated with the antibodies used for immunoprecipitation, proving that MID1-FLAG had been pulled down with anti-FLAG (Figure 3.2B-upper lane) and α4-myc with anti-myc (Figure 3.2C-lower lane).

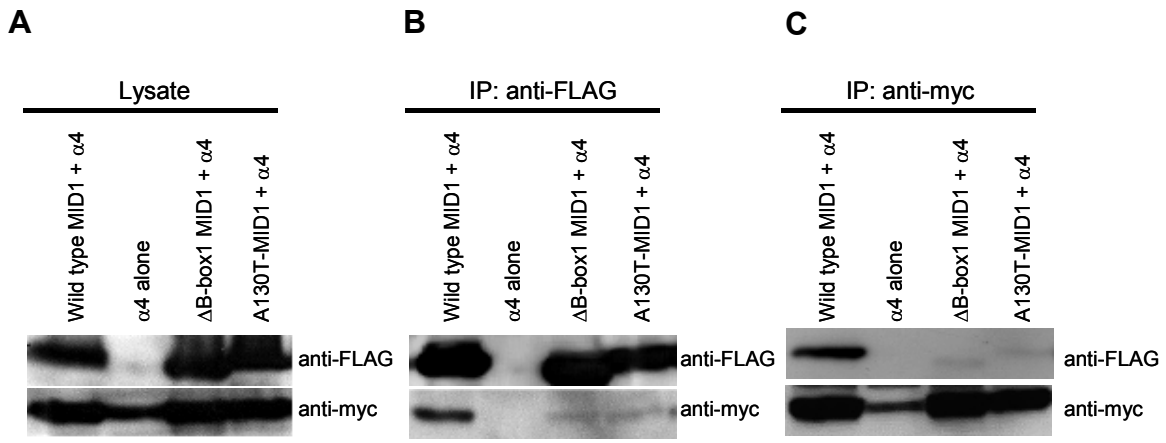

Figure 3.2. MID1 with altered Bbox1 do not co-immunoprecipitate with α4
A. COS-7 cells were transfected with wild-type MID1-FLAG or FLAG-tagged MID1 constructs lacking Bbox1 or carrying an A130T mutation and α4-myc. As background control, α4-myc was overexpressed alone. Cell lysates were separated on an SDS-gel, blotted and probed with anti-FLAG (upper line) and anti-myc (lower lane). **B**. Immunoprecipitation of MID1 constructs with anti-FLAG antibody. Precipitates were separated on an SDS-PAGE gel, blotted and probed with anti-FLAG (upper line) or anti-myc (lower lane). **C**. Immunoprecipitation of α4 with anti-myc antibody. Precipitates were separated on an SDS-PAGE gel, blotted and probed with anti-FLAG (upper lane) or anti- myc (lower lane).

In addition, yeast two-hybrid experiments based on β-galatosidase activity measurements were performed to quantify the putative binding affinities of different Bbox1 mutants to α4. Different MID1 constructs in pBMT116 vector, corresponding to wild-type, A130T, C145S and ΔBbox1, were used as baits to screen for interaction with the α4 protein cloned in pGAD10. A cut-off value of 5 β-galactosidase units was defined, and measurements above this value were

considered as clear interaction. Accordingly, measurements below 5 units were considered as no interaction.

With β-galactosidase measurements below 5 units, both mutants (C145S and A130T), as well as the construct lacking Bbox1, did not interact with α4 (Figure 3.3), while wild-type MID1 showed clear interaction. This data fully supported the results of the immunofluorescence and immunoprecipitation experiments, confirming that mutations in the Bbox1 domain of MID1 disrupt the interaction of the protein with α4 and that Bbox1 is responsible for the interaction between MID1 and α4.

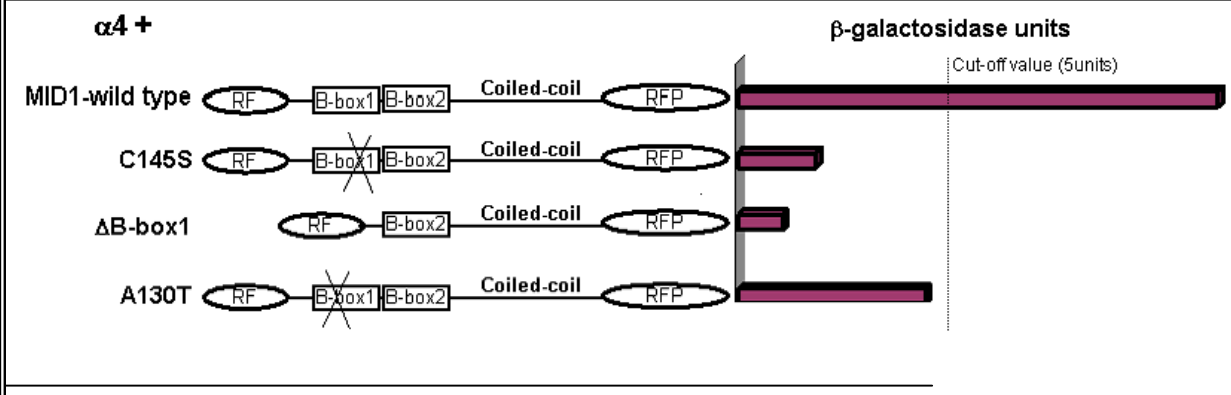

Figure 3.3. Yeast two-hybrid analysis of Bbox1 mutant's interaction to α4
The strength of the interaction between α4 and the indicated constructs was quantified by measuring the activity of a β-gal reporter. A cut-off value of 5 units, indicating the value above which clear interaction is considered, is marked with a dashed line.

3.1.2 Analysis of the structure of the Bbox2 domain

In addition to the OS related mutations described in Bbox1, one mutation has been identified so far in the Bbox2 domain of MID1 in an OS patient (De Falco et al., 2003). However, the effects of such mutations on the MID1 protein function have not yet been studied. Additionally, previous experiments in our group have shown that a mutated form of MID1 harbouring a single amino acid change in Bbox2, glutamine to arginine at position 192 (Q192R), while binding to microtubules, is unable to co-localise with α4 *in vivo*. Since Bbox1 alone is sufficient for MID1 to interact with α4, Bbox2 was proposed to act as a regulator of this interaction (Winter, 2003).

A first theoretical impression of the importance of these residues (Q192 and C195) in Bbox2 with respect to the structure of the domain, was acquired by comparison with a model of a previously reported *Xenopus* Bbox (Borden et al., 1995b). As outlined in the introduction section, Bboxes contain seven conserved histidines or cysteines and is arranged in a particular fashion, having two perpendicular β-strands connected by a flexible loop (Figure 3.4B) and a hydrophobic core. Four of the conserved Cys/His bind one zinc atom, as indicated

in figures 3.4B and 3.4C (sphere). According to this arrangement, it was predicted that C195 in MID1 Bbox2 (indicated with an arrow in Figure 3.4C) would form a part of the conserved core of residues, and that it is placed in the flexible loop of the domain. This structure has been proposed to probably participate in the correct positioning of the coiled-coil domain and, subsequently, the C-terminal end of MID1 (Borden et al., 1995b). Evolutionary conservation confirms the predicted important structural roles of this residue (Khuri et al., 2001; Mnayer et al., 2005). Interestingly, while also located in the above described loop, Q192 was not found to be a conserved residue.

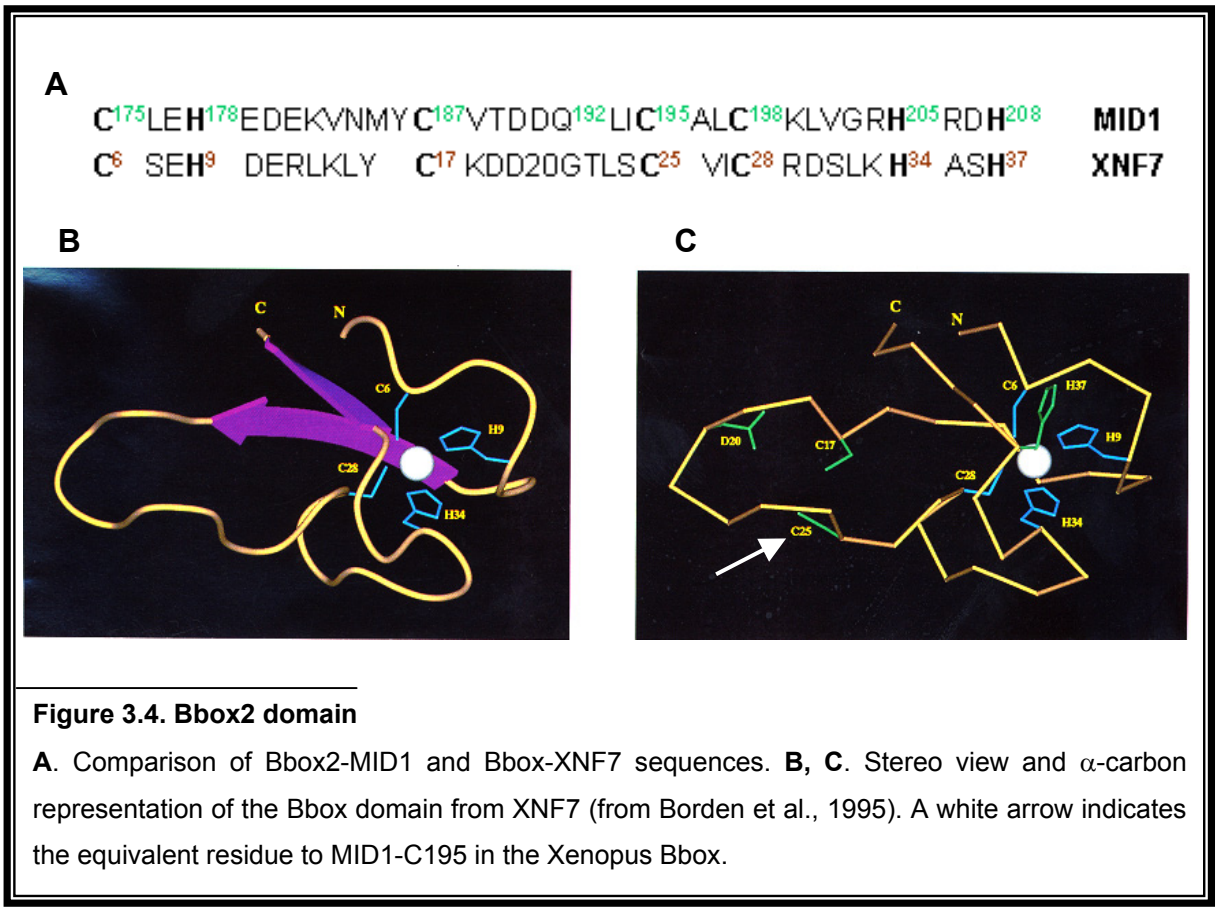

Figure 3.4. Bbox2 domain

A. Comparison of Bbox2-MID1 and Bbox-XNF7 sequences. **B, C**. Stereo view and α-carbon representation of the Bbox domain from XNF7 (from Borden et al., 1995). A white arrow indicates the equivalent residue to MID1-C195 in the Xenopus Bbox.

3.1.3 C195F, mutated MID1 form found in an OS patient, disrupts MID1-α4 interaction

In order to test for putative consequences of a mutation such as C195F in Bbox2 with respect to the association of MID1 to α4 *in vivo*, N-terminally GFP-tagged C195F-MID1 was overexpressed in COS-7 cells together with V5-tagged α4. Subcellular localization of both proteins was subsequently assayed by immunostaining as previously described. Confirming predictions, C195F-MID1 mutant protein not only lost α4 binding properties, but also its microtubule-binding affinity, probably due to major structural changes of the entire protein. In immunostained cells, while α4 appeared diffusely distributed in the cytosol, C195F mutant

protein accumulated in cytosolic aggregates (Figure 3.5A). The pictures clearly prove a loss of interaction of the two proteins, α4 and C195F MID1 *in vivo*.

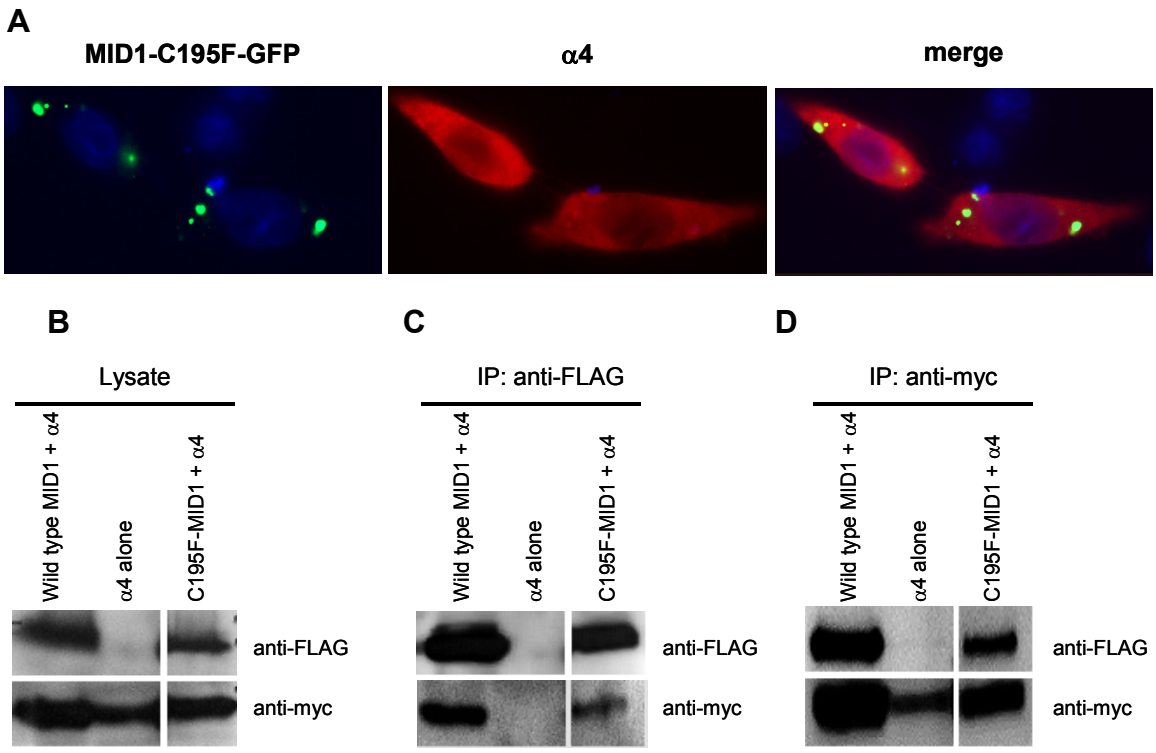

Figure 3.5. C195F-MID1 and α4 association

A. COS-7 cells co-expressing C195F mutated GFP-MID1 and V5-α4 (GFP-MID1 in green and V5-α4 in red). The nucleus is stained in blue with DAPI. **B**. Western blots showing the presence of the indicated constructs overexpressed in COS-7 cells **C**. Immunoprecipitation of MID1 constructs (wild-type, C195F and empty sample) with anti-FLAG antibody. Precipitates were separated on a SDS-PAGE gel, blotted and probed with anti-FLAG (upper lane) or anti-c-myc (lower lane) **D**. Immunoprecipitation of α4 with anti-myc antibody. Precipitates were separated on a SDS-PAGE gel, blotted and probed with anti-FLAG (upper lane) or anti-c-myc (lower lane).

For further research, immunoprecipitation experiments were performed with cytosolic extract from COS-7 cells co-expressing FLAG-tagged C195F-MID1 and α4-myc (Figure 3.5B). Immunoprecipitation with anti-FLAG and subsequent Western blotting of the precipitates with anti-myc, showed that both wild-type and C195F mutated MID1 interact with α4 *in vitro* (Figure 3.5C-lower lane). Similarly, a clear MID1 band was seen in both samples wild-type and C195F-mutant after immunoprecipitation of α4 with anti-myc and anti-FLAG incubation of the Western blots of the precipitates (Figure 3.5D-upper lane). Both blots were also incubated with the antibodies used for immunoprecipitation, confirming the efficiency of the precipitation reactions (Figure 3.5C-upper lane, Figure 3.5D-lower lane). In other words, unexpectedly,

these data indicate that while not being strong enough to disrupt the interaction of Bbox1 with α4 *in vitro*, a mutation such as C195 into F leads to misplacement and missfolding of MID1 that, consequently, can no longer interact with α4 *in vivo*.

3.1.4 Bbox2 mutants do not interact with α4 *in vivo*

All observations made thus far pointed towards a relevant structural and functional role for the Bbox2 domain of MID1, which would not only play a important role in the interaction of MID1 with α4 but also with microtubules. To further characterise the function of this domain, site directed mutagenesis of selected amino acids was performed, and the influence of these mutations on the known functional abilities (α4- and microtubule-binding) of MID1 was studied. Mutated residues were chosen according to their putative effect on the MID1 structure predicted by comparison with the 3D-structure of XNF7 Bbox and the Bbox2 consensus sequence.

The following N-terminally GFP-tagged MID1 constructs were used in this study:

C175A: Cysteine-175 is located at the N-terminal end of Bbox2 and immediately precedes a loop/turn. It is conserved and participates in zinc binding. It was mutated into alanine, a hydrophobic amino acid.

C198A: Cysteine-198 is located in the flexible turn. It is conserved and participates in zinc binding. It was also mutated into alanine.

H178Y: Histdine-178 is located in the middle of the N-terminal loop. It is conserved and participates in zinc binding. It was mutated into tyrosine, another polar amino acid that contains an aromatic ring.

V183T: Valine-183, a hydrophobic amino acid would be the first amino acid of the first β-strand. It was mutated into threonine, a polar amino acid.

Q192R: Glutamine-192, a polar hydrophilic residue would be located at the loop region. It was mutated into arginine, a basic amino acid.

ΔBbox2: deletion of the entire Bbox2 domain.

ΔRing: deletion of the RING finger domain.

ΔRing-Bboxes: deletion of the RING finger domain and both Bboxes.

Splice variant-*Ex2d.7:* MID1 splice variant which has been shown to bind α4 more strongly than full-length MID1 (Winter et al., 2004).

Splice variant-*Ex2d.7*-C175A*:* splice variant with a C175A mutation in Bbox2.

Splice variant-*Ex2d.7*-H178Y: splice variant with a H178Y mutation in Bbox2.

Immunostaining experiments were performed in the same manner as described previously; the different GFP-MID1 constructs were co-expressed with α4-V5 in COS-7 cells and analysed by immunostaining (GFP-MID1 in green and α4-V5 in red). Like the OS mutant

C195F, the missense mutations C175A, C198A, H178Y and the deletion of the entire Bbox2, all of which are predicted to have drastic structural effects on the MID1 protein, produce aggregates that hardly interact with microtubules and do not interact with α4 (Figure 3.6A). In contrast, V183T and Q192R, non-conserved residues that are expected not to have such as significant effect on the MID1 protein structure as the previous mutations, showed a clear interaction with microtubules, but not with α4.

The splice variant *Ex2.d7* has been previously shown to have much higher binding affinity to α4 than full length MID1 in a ß-galactosidase based yeast two-hybrid assay, and therefore, it was proposed to participate in the regulation of the MID1 protein function (Winter et al., 2004). This splice variant has a protein truncation stop signal after the coiled-coil domain and, in addition, exon1 is shortened, therefore losing most of the Bbox2 domain (only the seven first amino acids of the domain are kept).

Ex2d.7 does not interact with microtubules but appears diffusely distributed similar to α4, although they both seem to co-localise, as previously reported (Winter et al., 2004). In this case, none of the mutations, C175A or H178Y, contained in the Bbox2 part seemed to have strong effects; localisation of the protein was not modified and no clumps were formed (Figure 3.6B, middle and lower panels). However, as both proteins showed diffuse pattern in the cytosol, it was difficult to charge if they interact by immunofluorescence. For this reason, ß-galactosidase based yeast two-hybrid assays were also performed (see below).

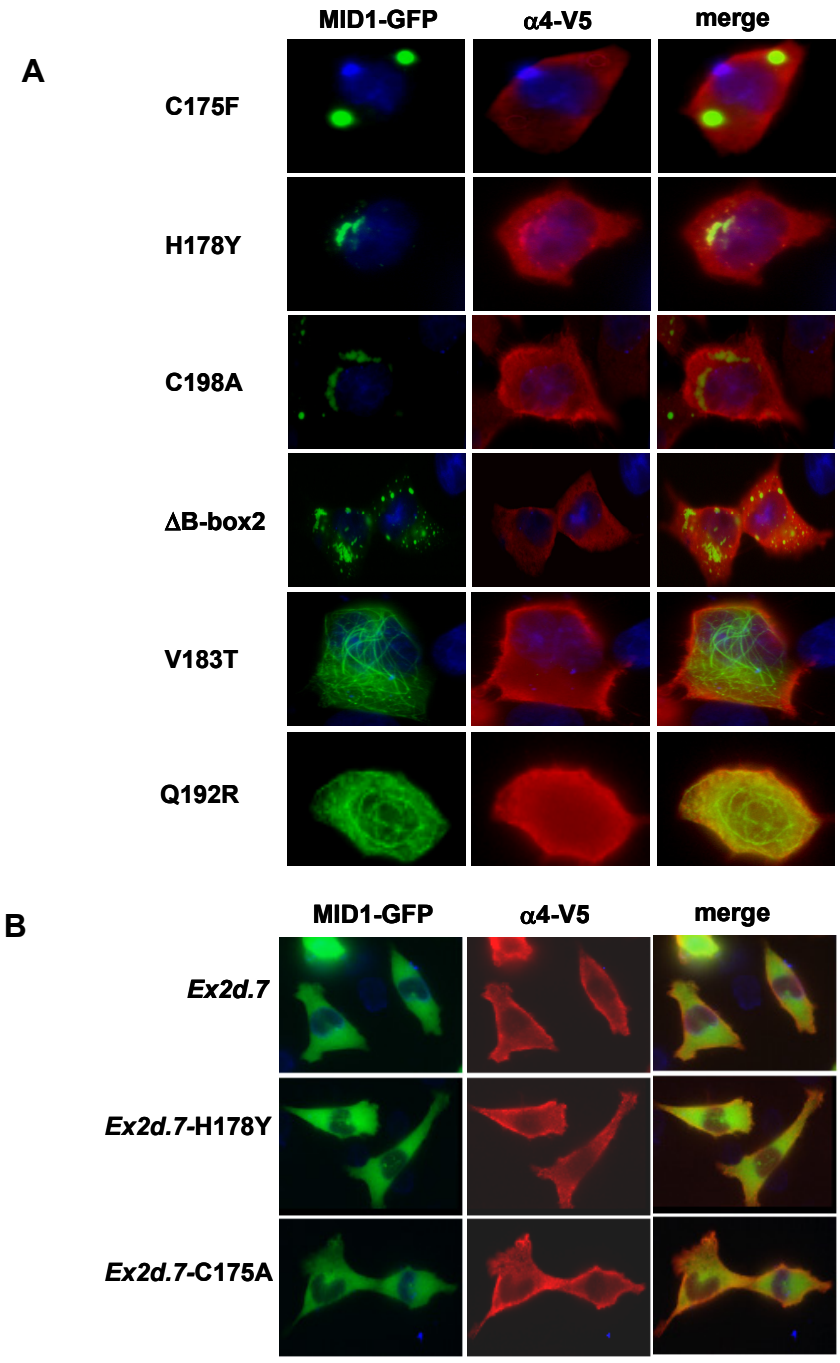

Figure 3.6. Bbox2 mutants do not interact with Bbox2 *in vivo*

A. COS-7 cells co-expressing different MID1 constructs with mutations in the Bbox2 domain or the complete deletion of the domain and α4 were immunostained. GFP shows the localisation of MID1 in green, and α4 is labelled in red with Cy3. Merge signals are shown to the right Nuclei are visualized in blue with DAPI staining. **B**. Constructs carrying the Ex2d.7 splice variant without or with mutations (C175A, H178Y) were examined in the same way.

Most of the Bbox2 mutants, as well as the deletions of any of the Bboxes, exhibited difficulties to interact with microtubules, suggesting that not only an intact C-terminus but also the Bboxes are essential for the correct folding and positioning of MID1 at the microtubules. It has previously been shown that mutations in the coiled-coil domain do not misplace MID1 or affect its interaction with α4. A mutated C-terminal domain, while abolishing microtubule-association, has also no influence on α4 binding (Liu et al., 2001; Schweiger et al., 1999; Trockenbacher et al., 2001). However, no data about putative effects of the RNG finger domain are available yet. Thus, a MID1 construct lacking the RING domain and a second one lacking the RING and the Bboxes domains were examined by immunostaining for microtubule-association. In addition, the α4 binding properties of the construct lacking exclusively the RING were studied. It was observed that, while the absence of the RING did not have any effect on the position of MID1 at the microtubules or its binding with α4, the additional absence of the Bboxes led to misplacement of the protein (Figure 3.7). This result confirms again that the Bboxes are necessary not only for proper α4 interaction (as shown in sections 3.1.1 and 3.1.4), but also for providing the correct emplacement of MID1 at the microtubules, even when the C-terminal end of the protein remains unaltered.

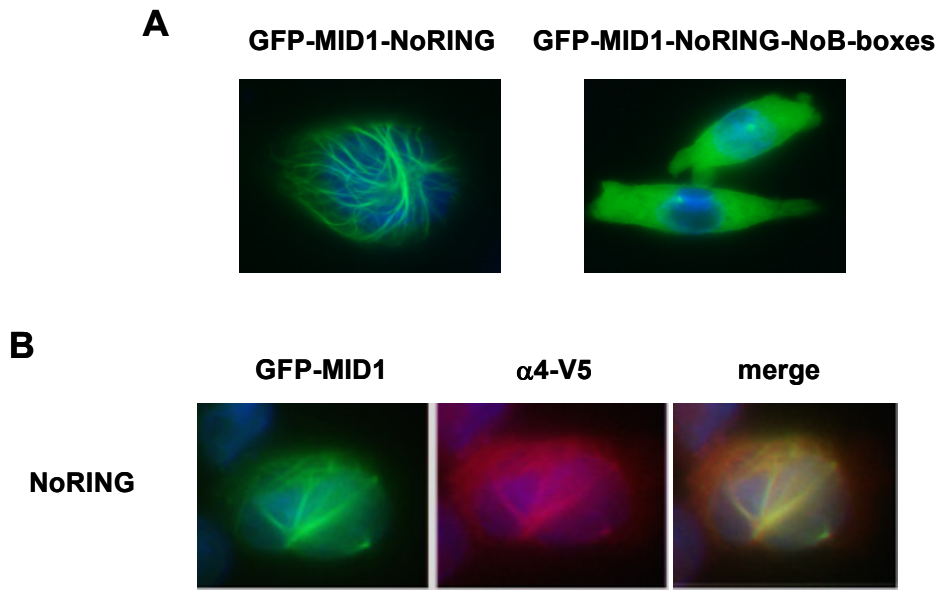

Figure 3.7. RING domain

A. COS-7 cells overexpressing MID1 constructs lacking the RING domain or the RING domain and the two Bboxes. GFP-tag confers MID1 green colour. **B**. Co-expression of a GFP-MID1 construct lacking the RING finger domain (in green) and α4-V5 (in red). Merge signal is shown to the right. Nuclei are visualized in blue with DAPI staining.

3.1.5 Bbox2 mutants interact with α4 *in vitro*

Further characterisation of a putative interaction of Bbox2 MID1 mutants with α4 required a study of the *in vitro* situation, which would help to clarify whether Bbox2 mutants do not interact with α4 *in vivo* because they are not well positioned, or because the interface of the α4 binding site is affected. Immunoprecipitation experiments with anti-myc antibody were performed with different N-terminally FLAG-tagged Bbox2 mutants co-expressed with myc-tagged α4 in COS7-cells (Figure 3.8A). Apart from a MID1 construct lacking the entire Bbox2 and the previously described constructs carrying point mutations in the Bbox2 domain, a construct including only the first seven amino acids of the domain, resembling the earlier

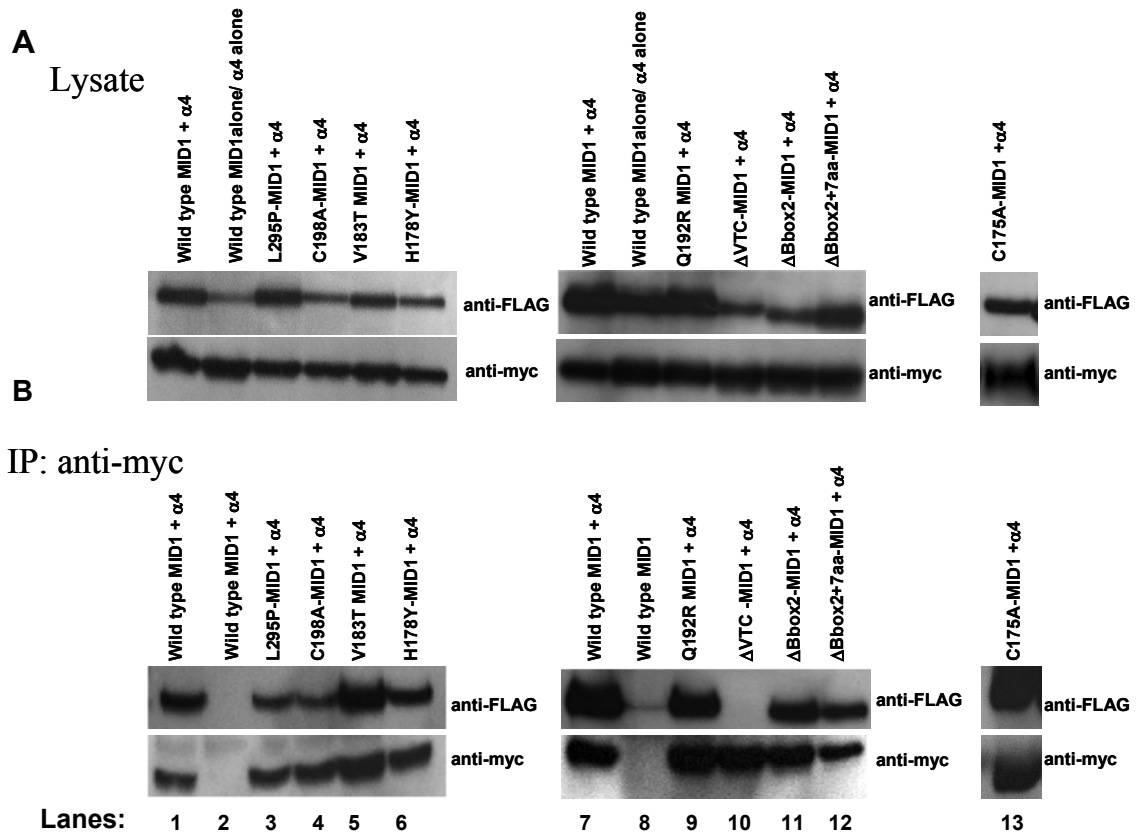

Figure 3.8. Co-immunoprecipitation of Bbox2 mutated constructs with α4

A. Western blots showing the presence of the indicated construct overexpressed in COS-7 cells. Note: lanes 2 and 8, upper panel shows overexpression of MID1-FLAG alone and the lower panel α4 alone **B.** Immunoprecipitation of MID1 constructs carrying mutations in Bbox2, in Bbox1 (ΔVTC, lane 10) or in the coiled-coil domain (L295P, lane 3) with anti-myc antibody. Precipitates were separated on a SDS-PAGE gel, blotted and probed with anti-FLAG (upper line) or anti-myc (lower line). Control immunoprecipitation with anti-myc was done with the sample containing only MID1.

described splice variant (section 3.1.4) was included. A construct carrying the mutation ΔVTC

in Bbox1 was included as negative control for MID1-α4 binding. As positive control, a construct carrying a mutation in the coiled-coil domain, L295P (So et al., 2005), that was previously shown not to interfere with α4 binding (Schweiger et al, unpublished data), was used. Western blots developed with anti-FLAG antibody and with anti-myc antibody proved the efficiency of the precipitation reaction. Samples only expressing FLAG-tagged wild-type MID1 were used as background control.

As expected, the construct carrying a mutation in Bbox1 (ΔVTC) did not interact with α4, agreeing with the results from section 3.1.1 (Figure 3.8B-lane10), and the L295P mutation maintained unaltered its association with α4 (Figure 3.8B-lane3). Similarly to what was observed for the C195F mutant, all the Bbox2 mutants studied (C198A, V183T, H178Y, Q192R, C175A and deletion of Bbox with and without extra seven amino acids) were able to interact with α4 *in vitro* (Figure 3.8B-lanes 4,5,6,9,11,12,13), associating to α4 with similar intensity as L295P.

For further characterisation, β-galactosidase activity was measured in yeast two-hybrid assays to quantify the strength of the interaction between the different constructs and α4. Similarly to what was done for the Bbox1, a cut-off value at 5 units β-galactosidase activity was assigned. Measurements above this value were considered as interaction between the MID1 construct and α4. In confirmation with all the *in vitro* immunoprecipitation results obtained, all constructs tested were able to interact with α4 in the yeast system (Figure 3.9). The splice variant, *Ex2d.7* with and without C175A mutation, was also tested and showed higher binding affinity than all the other constructs (Figure 3.9). However, since unexpectedly all the Bbox2 mutated constructs interact with α4 *in vitro* and given that both splice variant and α4 are spread in the cytosol in immunofluorescence experiments, at this point it is not possible to make conclusions about the interaction of this splice variant with α4 *in vivo*.

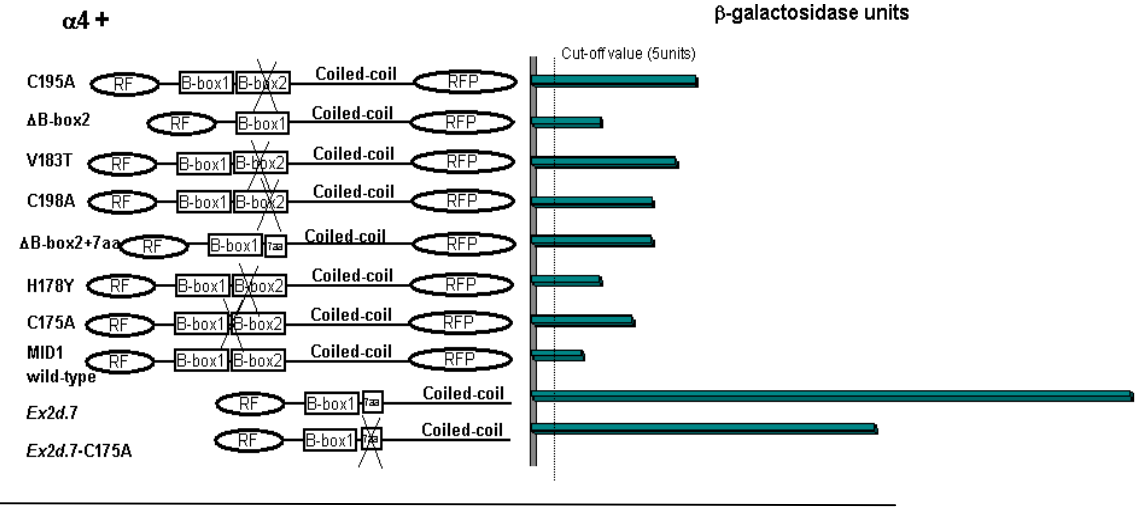

Figure 3.9. Yeast two-hybrid analysis of Bbox2 mutants -α4 interaction

The strength of the interaction between α4 and the indicated constructs was quantified by measuring the activity of a β-galactosidase reporter. A cut-off value of 5 units, indicating the value above which clear interaction is considered, is marked with a dashed line.

In summary, the results obtained during this thesis show that the Bbox2 domain considerably influences the interaction between α4 and MID1 *in vivo*. Single point mutations lead to complete disruption of this interaction *in vivo* but not *in vitro*. Furthermore, amino acid changes in the conserved core of amino acids in Bbox2 appear to affect the protein to a greater extent and lead to dissociation of the mutant protein from the microtubules, and disruption of the interaction between MID1 and α4.

3.2 Characterisation of the MID1 multiprotein complex

The elucidation of previously reported multiprotein complexes has allowed a much better understanding of the function of their main component proteins. Well-characterised examples are PML, FMRP or Staufen (Brendel et al., 2004; Ceman et al., 1999; Hodges et al., 1998; Sternsdorf et al., 1997). As mentioned earlier, MID1 forms part of a macromolecular complex, the composition of which was mainly unknown. Therefore, the elucidation of its components could shed light on different functions in which MID1 might be involved.

In this thesis, affinity chromatography was the method of choice to identify protein components of the macromolecular MID1 complex. For the preparation of the chromatography column, a peptide that was recombinantly produced in *E.coli* in a PinPoint vector system was used (see section 3.2.2). This peptide covered the MID1 binding region in the α4 protein, which had been recently narrowed down to 44 amino acids (44aa peptide) (Figure 3.10; R. Schneider and A. Köhler, unpublished data). Unfortunately, MID1 could not be used for the preparation of the column, as it contains many cysteines that impede the correct folding of the protein in *E.coli*.

237-PPVKPFILTRNMAQAKVFGAGYPSLPTMTVSDWYEQHRKYGAL-280

Figure 3.10. α4 peptide
44 amino acids peptide corresponding to the region of α4 that specifically interacts with MID1.

3.2.1 44aa peptide of α4 production in the PET32a vector system

Conditions for the expression of the 44aa peptide in *E.coli* were first established with the PET32a vector system, a very efficient protein expression system. Moreover, with this vector a His-tag suitable purification through Ni-NTA agarose and a Thioredoxin tag and a S-Tag that improve the solubility of the peptide could be incorporated to the peptide (Figure 3.12A). Several temperatures and concentrations of IPTG for induction of protein expression were tested in order to establish optimal conditions in the BL21 strain of *E.coli* (Figure 3.11, induction conditions). An aliquot of each culture was lysed under denaturing conditions with SDS-PAGE buffer or magic mix and analysed on a 15 % Coomassie stained SDS gel (Figure 3.11A). Having observed no difference in any of the tested conditions 2 h after induction, the minimum amount of IPTG (0.1 mM) at 37°C were taken as the conditions of choice. To test the solubility of the peptide produced under those conditions, cells were lysed in native conditions lysis buffer (see Methods section), and the soluble fraction was separated from

the insoluble by centrifugation at 10000 x g. Aliquots of the soluble and insoluble fractions, as well as induced and non-induced cells (lysed with SDS buffer), were analysed on a 15% Coomassie gel, and it was confirmed that the peptide was soluble under native conditions (Figure 3.11B). Subsequently, the peptide was purified through Ni-NTA and aliquots of each fraction (flow through, washes and elutions) were run on a 15% Coomassie stained SDS gel (Figure 3.11C).

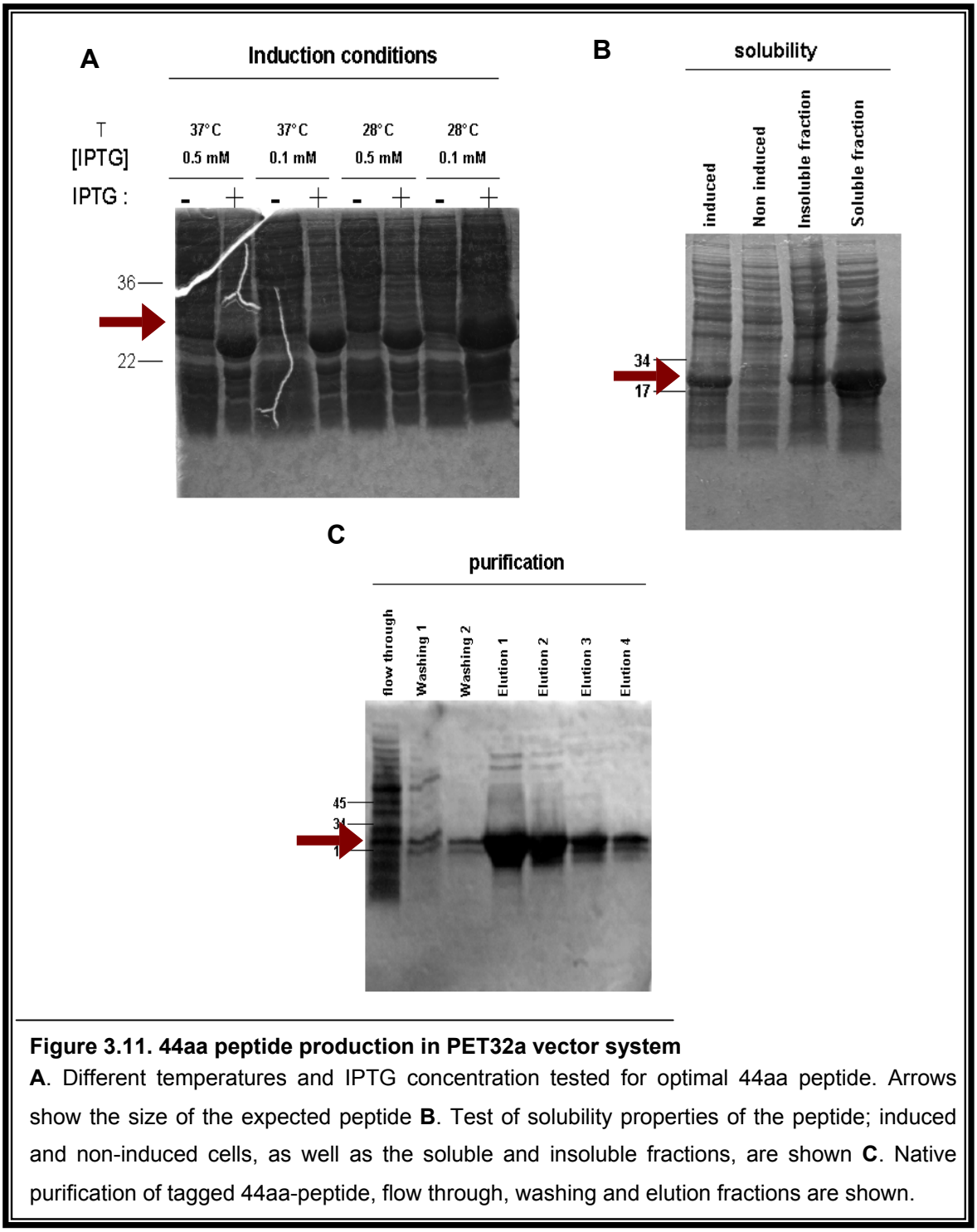

Figure 3.11. 44aa peptide production in PET32a vector system

A. Different temperatures and IPTG concentration tested for optimal 44aa peptide. Arrows show the size of the expected peptide **B**. Test of solubility properties of the peptide; induced and non-induced cells, as well as the soluble and insoluble fractions, are shown **C**. Native purification of tagged 44aa-peptide, flow through, washing and elution fractions are shown.

Although a stop codon had been introduced after the 44aa peptide coding sequence, the purified peptide presented with more than one band in the Coomassie gel (Figure 3.11C, Elutions 1-4). Therefore, the peptide was digested with thrombin in order to find out if the additional bands were degradation products, the result of translation from a later initiation codon or gel artefacts (Figure 3.12). Upon thrombin restriction, two bands of 14,7 kDa and 7,8 kDa were expected, and variations on the sizes of the obtained bands would indicate the source of the additional bands. Different conditions, including different incubation times and enzyme concentration, were tested for optimal digestion of the purified peptide at 4°C (Figure 3.12B). Samples were run on 15% SDS gels and silver stained. While the control experiment without enzyme remained intact, after 2 hours most of the peptide had been already digested with all enzyme concentrations tested. Interestingly, thrombin digestion resulted in two well-defined bands at the expected sizes (green arrows), confirming that the additional bands

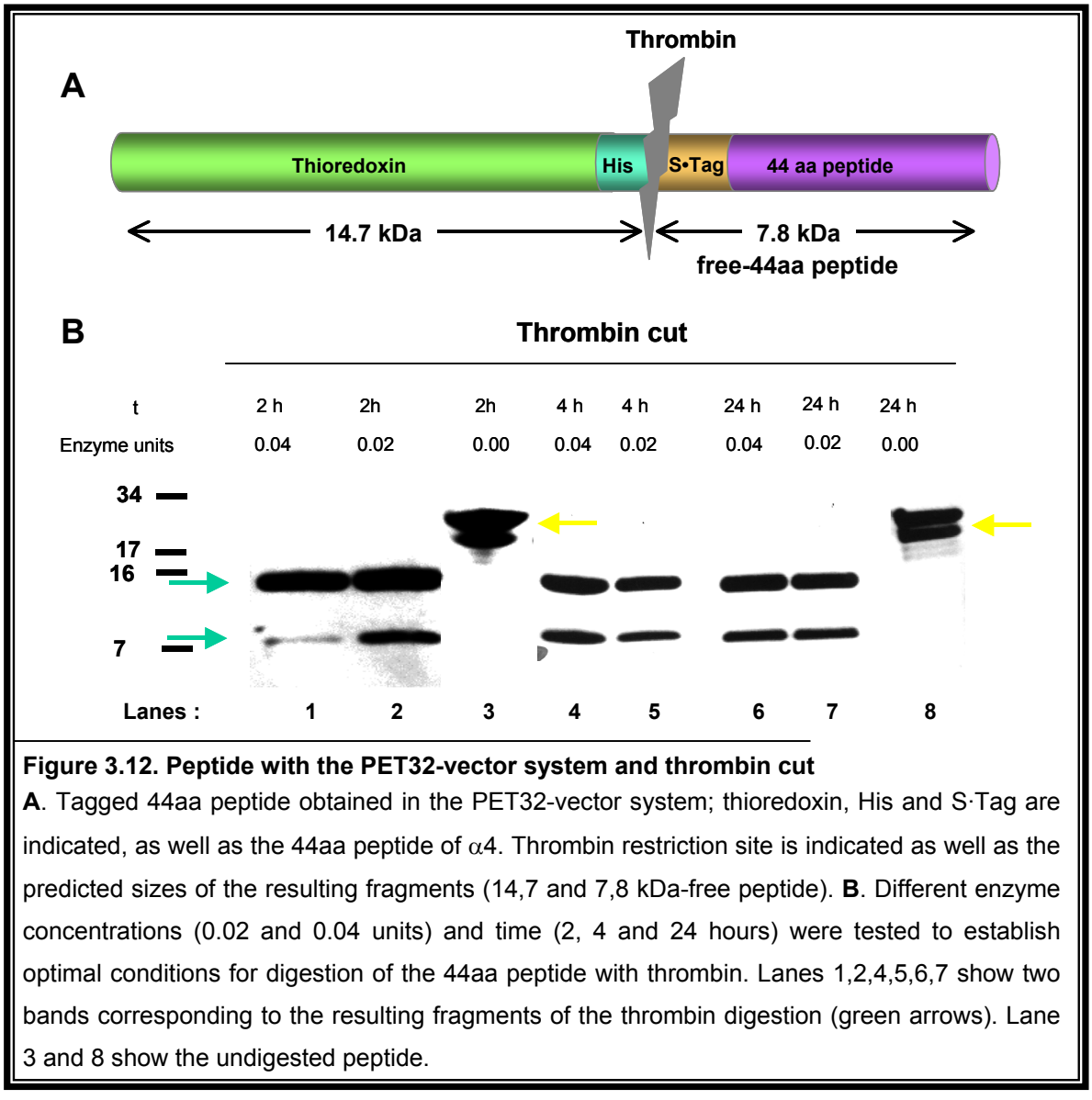

Figure 3.12. Peptide with the PET32-vector system and thrombin cut

A. Tagged 44aa peptide obtained in the PET32-vector system; thioredoxin, His and S·Tag are indicated, as well as the 44aa peptide of α4. Thrombin restriction site is indicated as well as the predicted sizes of the resulting fragments (14,7 and 7,8 kDa-free peptide). **B**. Different enzyme concentrations (0.02 and 0.04 units) and time (2, 4 and 24 hours) were tested to establish optimal conditions for digestion of the 44aa peptide with thrombin. Lanes 1,2,4,5,6,7 show two bands corresponding to the resulting fragments of the thrombin digestion (green arrows). Lane 3 and 8 show the undigested peptide.

observed in the undigested peptide are probably due to gel artefacts. No degradation of the undigested peptide (yellow arrows) was observed even after 24 hours at 4°C in untreated controls.

The free 44aa peptide was subsequently used for elution of the chromatography column (see below) and for that purpose, thrombin was used to cleave the thioredoxin-tag and the His-Tag as previously described (Figure 3.12A). The free 44aa peptide, only including the S-Tag, was recovered by trapping the fragment including the tags in Hepes sucrose buffer (HS buffer) equilibrated Ni-NTA agarose and collecting the flow through containing the 44aa peptide.

3.2.2 α4 peptide production in the PinPoint vector system

With the pinpoint vector system, a biotinylated peptide can be produced which can then be immobilized on streptavidin-coated agarose beads. Thus, the sequence corresponding to the 44aa peptide including a stop codon was cloned into the PinPoint -Xa vector, and a His-RGS tag was additionally included in order to purify the peptide through Ni-NTA agarose. To set up optimal expression time the biotinylated peptide was overexpressed in *E.coli* (strain JM109) in the presence of 2 μM biotin upon induction with 0.1 mM IPTG for one, two, three or four hours. An aliquot from each culture was run in a 15% SDS-PAGE gel and checked by Coomassie staining (Figure 3.13A). Although the approximately 22 kDa big peptide started to be expressed 2 hours after induction, at least three to four hours were necessary to obtain the highest expression levels. As a control, the same vector without the peptide was used, showing a similar induction pattern.

Having established the expression conditions, the peptide was purified through Ni-NTA agarose and its purity was tested on a 15% Coomassie gel (Figure 3.13B). Of note, two bands corresponding to the peptide were obtained, probably due to gel artefacts.

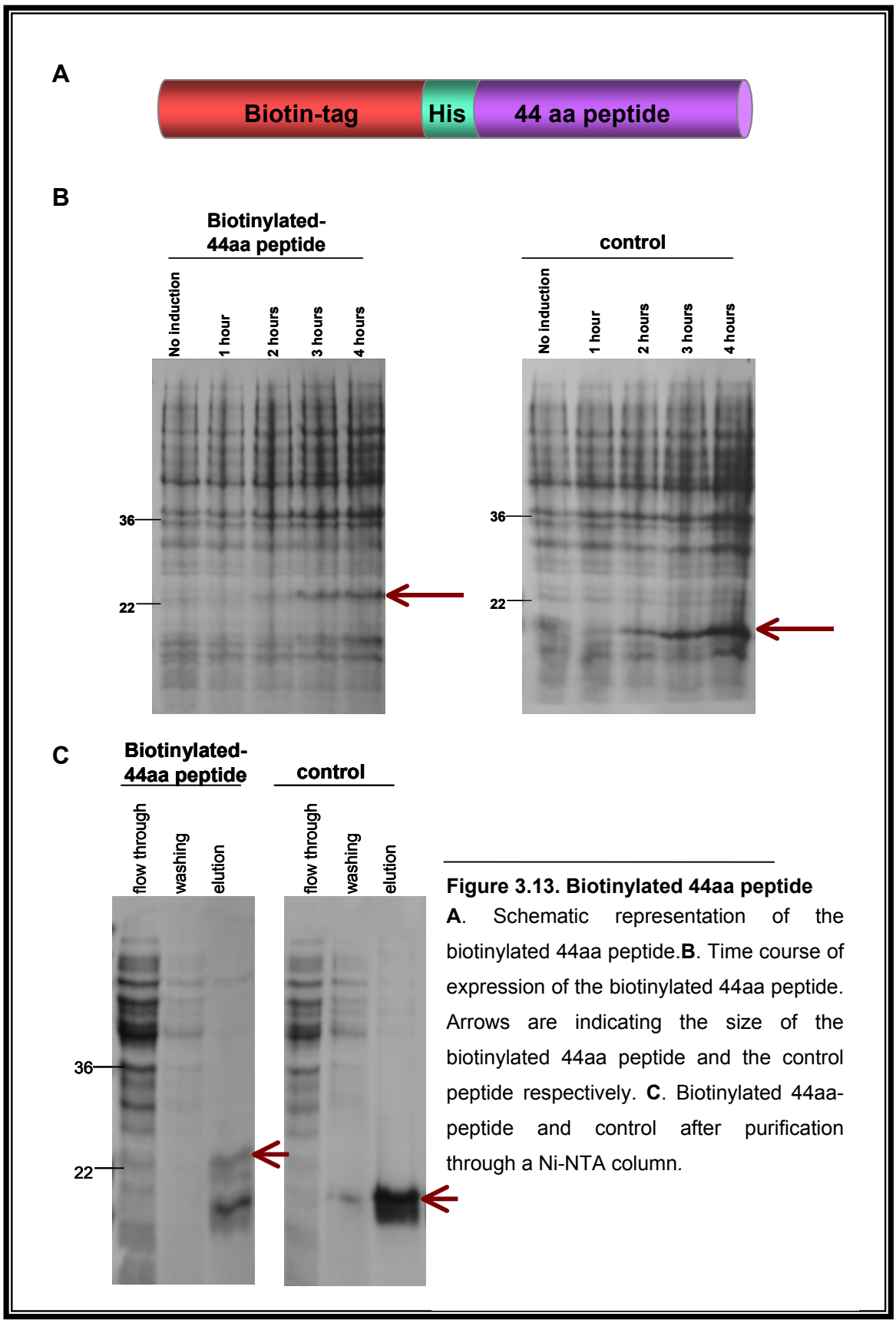

Figure 3.13. Biotinylated 44aa peptide
A. Schematic representation of the biotinylated 44aa peptide.**B**. Time course of expression of the biotinylated 44aa peptide. Arrows are indicating the size of the biotinylated 44aa peptide and the control peptide respectively. **C**. Biotinylated 44aa-peptide and control after purification through a Ni-NTA column.

3.2.3 Affinity chromatography column

For preparing the affinity chromatography, the biotinylated 44aa peptide was bound to streptavidin coated agarose beads and subsequently blocked with BSA to reduce unspecific interactions. In parallel, a control experiment without peptide was performed. After blocking, the columns were extensively washed first with free 44aa peptide and, then, with 100 volumes of HS buffer and 2 volumes of washing buffer (250 mM NaCl/0,05% Tween), followed by equilibration in HS buffer. Afterwards, cytosolic HeLa extracts were added to both columns (with and without peptide). In order to avoid competition for MID1 between endogenous α4 and the biotinylated 44aa peptide bound to the column, endogenous α4 had been previously knocked-down by siRNA (Figure 3.14).

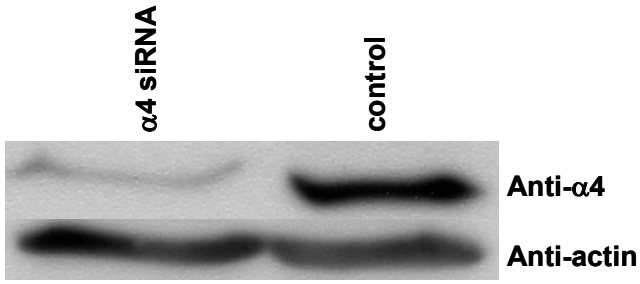

Figure 3.14. α4 knock-down
Western blots of HeLa cell lysates after α4 knock down or a control experiment without siRNA. Endogenous anti-α4 antibody was used for detection. Incubation with anti-actin confirmed equal protein loading.

After extensive washing, MID1 and its interaction partners were eluted with free 44aa peptide (section 3.2.1). Eluted proteins were dialysed to remove the excess of peptide and analysed on a 10% SDS gel that was subsequently colloidal Coomassie stained. Bands absent in the control gel were cut out and analysed by electrospray ionisation mass spectrometry (ESI-MS). Figure 3.15 shows the colloidal Coomassie stained gel and the protein identities of the analysed bands, after correlation of the obtained peptides with the Swiss-Prot database.

Tubulin beta-5-chain identification (Figure 3.15) resembled microtubule binding ability of MID1 shown before in our lab (Schweiger et al., 1999) and served as a proof of specificity. In addition, several heat shock proteins, namely Heat shock protein HSP 90-beta (Hsp90), Heat shock cognate protein 71kDa protein (Hsc70) and 60 kDa heat shock protein (Hsc60), being Hsp90 the most abundant, were identified. Unfortunately, MID1 detection was hindered by a very strongly encountered E.*coli* heat shock protein (Heat shock protein 70, *E.coli*) that has the same molecular size and was also present in the control sample. In addition,

elongation factor 1-alpha1 (EF-1α), Annexin A2 (ANXA2), Q subcomponent binding protein (p32), RACK1, Nucleophosmin (NPM) and several ribosomal proteins of the small 40S subunit (S3, S8) were found. Table 1 shows a summary of already reported functions of the proteins identified after mass spectrometry.

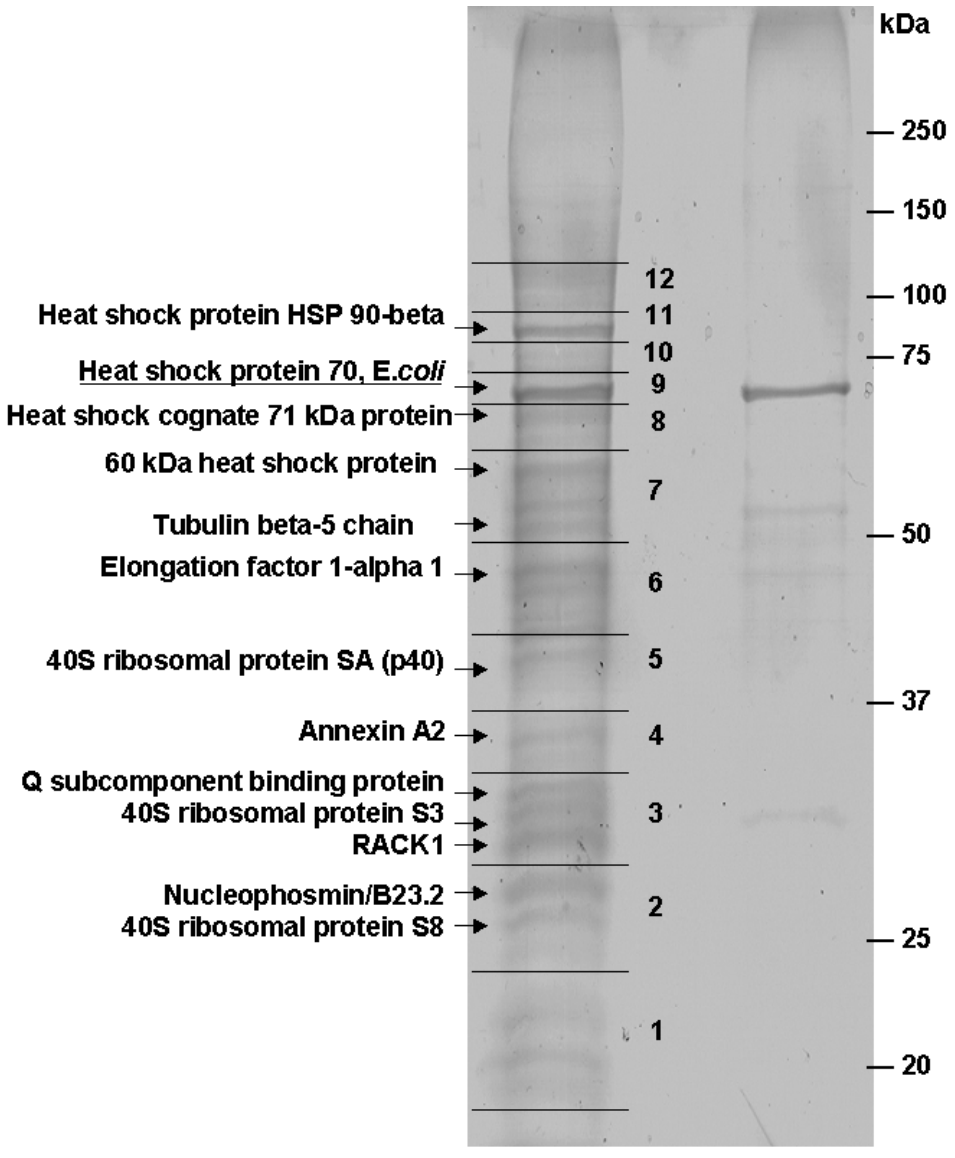

Figure 3.15. Colloidal coomassie results
Colloidal Commasie staining of proteins eluted from the chromatography column coated with biotinylated 44aa peptide (left lane) compared to the control column without peptide (right lane). Protein identities of the analysed band are given to the left.

Protein	Short name	Accession number	Function	References
Heat shock protein HSP90-beta	Hsp90	P08238	•*RNA binding protein* •*Cell cycle progression as chaperon of cell cycle regulation and Polo-like kinases* •*Centrosome duplication* •*Buffer of insulin-like growth factor and insuline signalling* •*Participates in the reduction of Huntingtin aggregates*	(Burrows et al., 2004; de Carcer, 2004; de Carcer et al., 2001; Lange et al., 2000; Meares et al., 2004; Nakai and Ishikawa, 2001; Sittler et al., 1998)
60 kDa heat shock protein	Hsc60	P10809	•*Chaperon* •*Mitochondrial functions* •*Regulation of stress-induced apoptosis*	(Bukau and Horwich, 1998; Gupta and Knowlton, 2005; Voos and Rottgers, 2002)
Heat shock cognate 71 kDa protein	Hsc70	P11142	•*Chaperon* •*Associates with Huntingtin aggregates*	(Jana et al., 2000)
Tubulin beta-5 chain or Tubulin beta-1	Tubulin	P05218	•*Monomer of microtubules* •*Microtubule dynamics*	(Cooper, 2000)
Elongation factor 1-alpha 1	EF-1α	P04720	•*Peptide chain elongation* •*Cytoskeleton regulation* •*Interaction with mitotic apparatus* •*Regulation of microtubules dynamics* •*Associates with Huntingtin aggregates*	(Condeelis, 1995; Mitsui et al., 2002; Moore R.C and R.J., 2000; Moore RC et al., 1998; Negrutskii and El'skaya, 1998; Ohta et al., 1990);
40S ribosomal protein SA (p40) (34/67 kDa laminin receptor)	SA	P08865	•*Tumor cell growth and proliferation* •*RNA processing and ribosome maturation*	(Ford et al., 1999)
Annexin A2	ANXA2	P07355	•*RNA-binding protein* •*Mediator of Ca2+ regulated endocytosis and exocytosis. Regulation of ion channels* •*DNA binding* •*Inhibition of cell adhesion*	(Balch and Dedman, 1997; Filipenko et al., 2004; Vedeler and Hollas, 2000)

Protein	Short name	Accession number	Function	References
Receptor for activated C kinase 1	RACK1	P25388	• *RNA binding protein* • *Scaffold protein* • *Regulation of cycle progression* • *Constituent of the eukaryotic ribosomes.* • *Positioning of ribosomes where translation is required, eg. Focal adhesions* • *Regulation of STAT3 activation through insulin-like growth factor 1 and insuline signalling* • *Intracellular Ca2+ regulation* • *Regulation of integrin-mediated adhesion*	(Cox et al., 2003; Mamidipudi et al., 2004a; Mamidipudi et al., 2004b; McCahill et al., 2002; Nilsson et al., 2004; Sklan et al., 2006; Zhang et al., 2006)
40S ribosomal protein S3	S3	P23396	• *Constituent of the small ribosome subunit; DNA repair* • *Apoptosis/cell growth regulation*	(Jang et al., 2004; Stahl, 2001; Wittmann-Liebold and Graack 2001)
Q subcomponent binding protein	p32	Q07021	• *Chaperon – PKC μ regulatory protein* • *Mitochondrial oxidative phosphorylation* • *Splicing modulation*	(Chattopadhyay et al., 2004; Krainer et al., 1991; Storz et al., 2000)
40S ribosomal protein S8	S8	RS8_HUMAN	• *Constituent of the small ribosome subunit*	(Stahl, 2001; Wittmann-Liebold and Graack 2001)
Nucleophosmin/B2 3.2	NPM	Q9BYG9	• *RNA binding protein* • *Ribosome biogenesis* • *Regulation of transcription,* • *DNA replication and apoptosis Centrosome duplication* • *Cytoplasmic nuclear trafficking* • *Cancer pathogenesis* • *Pre mRNA processing*	(Fankhauser et al., 1991; Grisendi et al., 2005; Okuda, 2002; Shinmura et al., 2005; Tarapore et al., 2002; Tarapore et al., 2006; Wang et al., 1994);

Table 3.1 Previously reported functions of novel identified MID1 interaction partners

Name, short name, accession numbers from the Swiss-Prot data base and functions of the different identified MID1 interaction partners by MS are listed. References are also given.

3.2.4 Confirmation of novel MID1 interaction partners

In order to verify the association of the proteins identified by MS with MID1, co-immunoprecipitation experiments were performed with HeLa extracts overexpressing N-terminally FLAG tagged-MID1 (MID1-FLAG). Agarose-beads coated with anti-FLAG antibody were used to immunoprecipitate MID-FLAG, and bound proteins were specifically eluted with 3 x FLAG-peptide. Precipitated proteins were analysed on Western blots incubated with endogenous antibodies for the respective proteins and anti-FLAG to detect MID1-FLAG itself. As negative control, the same immunoprecipitation experiment was performed with cytosolic HeLa extracts without MID1-FLAG expression.

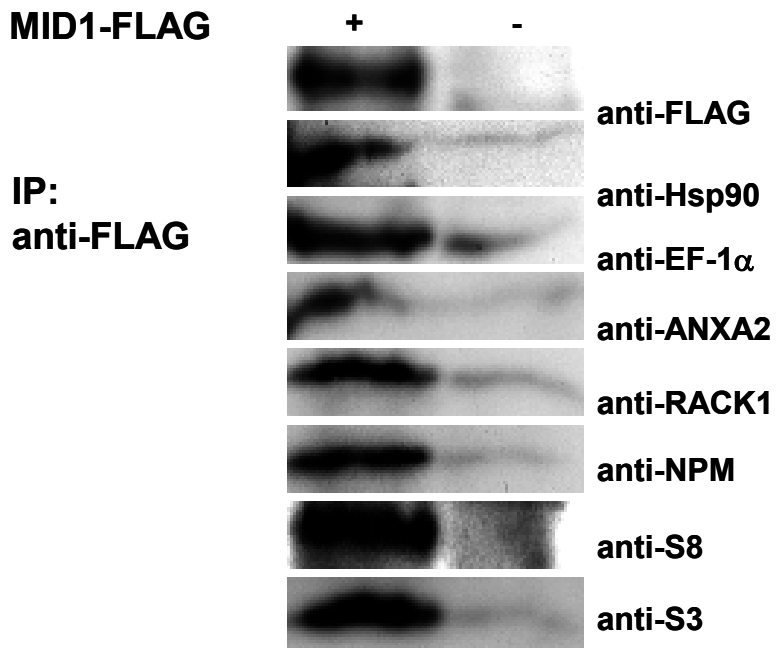

Figure 3.16. Co-immunoprecipitation of MID1-FLAG with the novel interaction partners
On the left lane precipitates of HeLa cells with MID1-FLAG overexpression were loaded and on the right lane, precipitates of HeLa cells without FLAG-MID1 overexpression. Antibodies used for Western-detection are given.

In the presence of MID1-FLAG, all the proteins studied could be pulled down with the anti-FLAG coated beads (Figure 3.16, left lane). On the contrary, in the control experiment only background binding was observed (Figure 3.16, right lane), confirming specific association of MID1 with the identified proteins.

3.2.5 The MID1 protein complex is found in purified microtubules

As mentioned previously, association of MID1 with microtubules has previously been demonstrated (Schweiger et al., 1999), which was again confirmed here by the identification

of Tubulin β-5 chain in the protein complex. In order to test whether the other components of the MID1 complex associate to microtubules as well, microtubules were purified from HeLa cells lysates through subsequent polymerisation/depolymerisation steps with taxol and carefully washed. The presence and enrichment of the different proteins in the pure microtubule fraction was tested on Western blots incubated with antibodies detecting the respective members of the complex. Bands in purified microtubules were compared to total HeLa cell lysates loaded with the same amounts of protein (Figure 3.17).

A tubulin α/β enrichment in the purified fraction compared to the lysate, indicated successful isolation of microtubules (Figure 3.17). An enrichment in S3, NPM and RACK1 was also observed, corroborating the interaction of the complex with microtubules. Moreover, considerable amounts of EF-1α and ANXA2 were found at the microtubules, although interaction of these proteins depends on Ca^{2+} and this factor was not considered. Finally, only small amounts of Hsp90 and Hsc70 were found in the microtubules fraction, indicating a weaker interaction of those proteins with the complex.

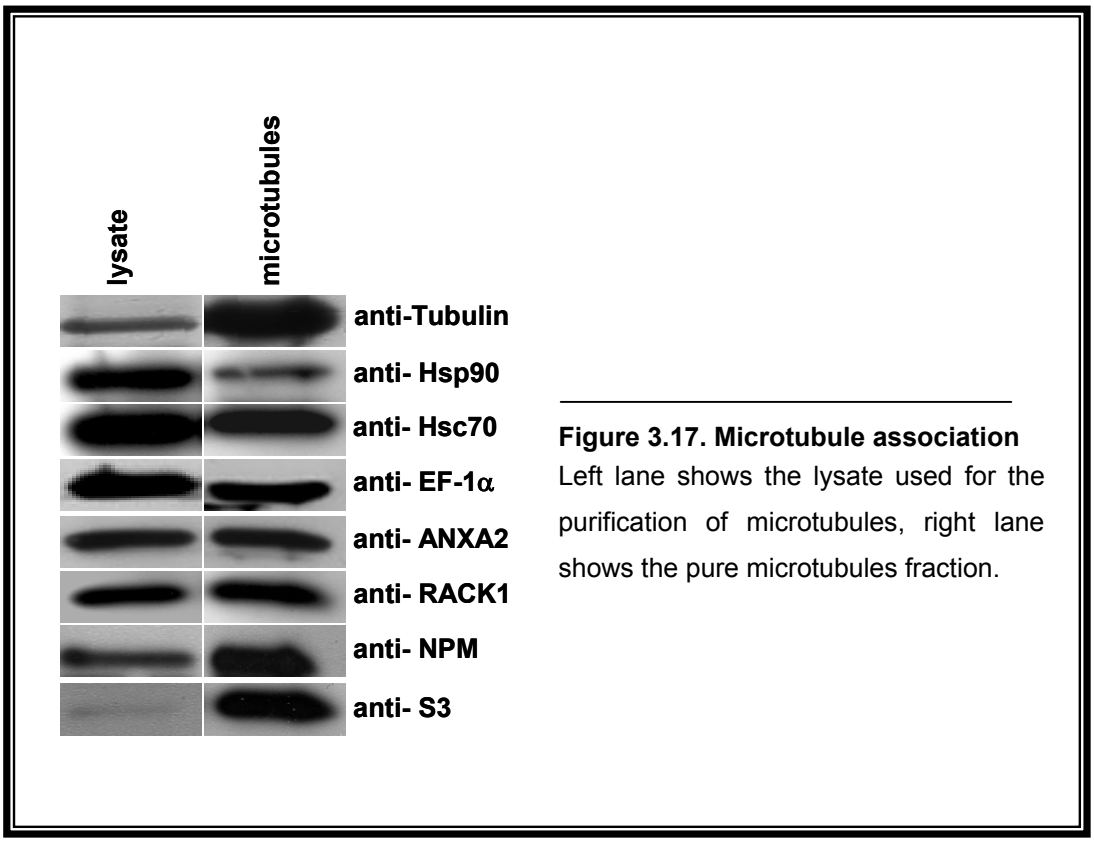

Figure 3.17. Microtubule association
Left lane shows the lysate used for the purification of microtubules, right lane shows the pure microtubules fraction.

3.2.6 The MID1 complex associates with both ribosomal subunits

Among the newly identified MID1 complex members, it was remarkable the presence of ribosome related proteins such as S3, S8, p40 and RACK1, which have been found to be constituents of the small ribosomal subunit. Additionally, EF-1α, an important member of the translation machinery, several heat shock proteins, NPM (involved in ribosome biogenesis) and

ANXA2 (another ribosome-associated protein) were found in the complex. All these data together indicated that the MID1 complex associates with ribosomes. However, interaction with the big ribosomal 60S subunit, had not been observed in the already performed experiments.

In order to test if the MID1 complex also associates with the big ribosomal subunit, MID1-FLAG overexpressed in HeLa cell lysates was immunoprecipitated with anti-FLAG antibody, following the same procedure as in section 3.2.4 Instead, this time MID1-FLAG immunoprecipitates were examined by Western blot for the presence of L5, a ribosomal protein component of the big ribosomal subunit 60S (Figure 3.18).

While only background binding was observed in the control sample (Figure 3.18, right

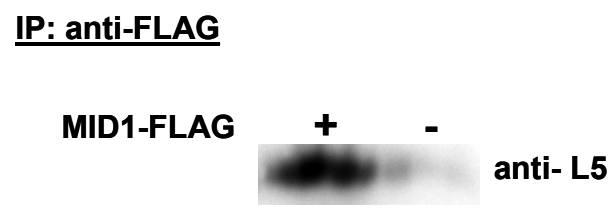

Figure 3.18. Association of FLAG-MID1 with the big ribosomal subunit, 60S
MID1-FLAG immunoprecipitates were examined for the presence of L5, member of the big ribosomal subunit. Immunoprecipitates from HeLa cells without MID1-FLAG overexpression were used as background control.

lane), clear co-immunoprecipitation of L5 and MID1-FLAG was seen in FLAG-MID1 overexpressing HeLa cells (Figure18, left lane). This result confirms the association of the MID1 protein complex with both ribosomal subunits.

3.2.7 MID1 associates with intact ribosomes

Previous experiments strongly indicated that the MID1 complex associates with ribosomes. To further characterise this association, HeLa cytosolic extracts overexpressing MID1-FLAG were run through discontinuous sucrose gradients (20%-50%) by ultracentrifugation in a fix-angle rotor to, consequently, separate the ribosomal fraction from the rest. Four distinct fractions of the resulting gradient were studied on Western blots developed with antibodies corresponding to the different members of MID1 complex. The first fraction was the top of the gradient with no sucrose, the second was the 20% sucrose layer, the third was the interface between the 20% and the 50% layer, and the ribosomal pellet resolved in urea and SDS containing magic-mix (see Method section) was the fourth fraction. The lysate was additionally loaded on the SDS gel.

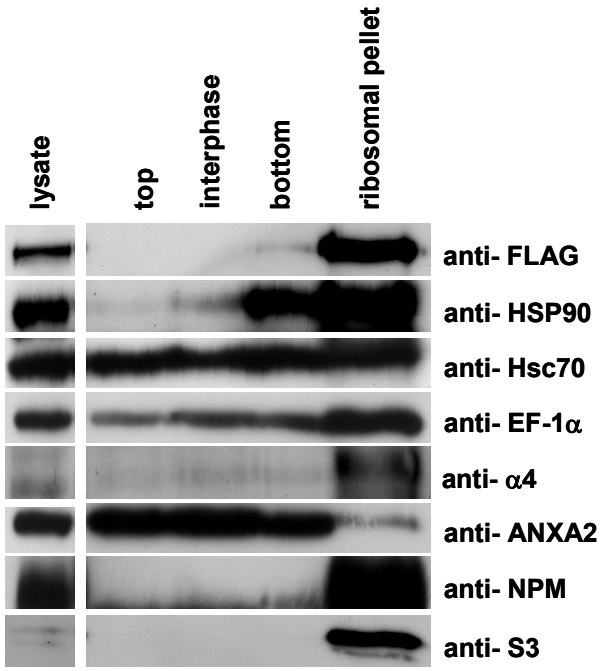

Figure 3.19. MID1 complex associates with ribosomes
Four different fractions of a 20%-50% discontinous sucrose gradient were loaded on SDS-gels together with the lysate used for the preparation (left lane), different antibodies were used for the detection of several members of the MID1 complex. Top: upper part of the gradient; Interphase: 20% sucrose layer; Bottom: interface between 20% and 50%. The ribosomal pellet is shown in the very right lane.

As shown in Figure 3.19, Hsp90, Hsc70, EF-1α, NPM, ANXA2, α4 and MID1-FLAG co-sediment in the ribosomal pellet, which is indicated by the presence of the ribosomal protein S3, another a member of the complex. However, not all the members of the complex showed the same affinity. α4, the best-characterised MID1 interaction partner, was mainly found in the ribosomal pellet together with MID1 and NPM. Other members of the complex, such as Hsc70, Hsp90 and EF-1α, were found in all the fractions, indicating that probably only a pool of those proteins associate with the MID1 complex and the ribosome. Interestingly, only small amounts of ANXA2 were found in the ribosomal pellet, which could be due to Ca^{2+} dependency of ANXA2 properties. All experiments described were performed under cold-shock conditions, so that microtubules remained depolymerised and could not pellet with the ribosomal fraction.

3.2.8 MID1 forms part of a ribonucleoprotein complex

Taking together that the MID1 complex associates with ribosomes and that some of the identified proteins are RNA binding protein or closely related to RNA (namely NPM, ANXA2,

RACK1), it was reasonable to think that the MID1 complex could be the core of a ribonucleoprotein (RNP) complex, composed of proteins and RNA.

To test this possibility, the influence of RNA on the association of the MID1 complex with ribosomes was assayed by running discontinuous 20%-50% sucrose gradients in a fixed-angle rotor with MID1-FLAG overexpressing cytosolic extracts, which were pre-treated with RNaseA, DnaseI or RNAguard (RNase inhibitor). Subsequently, Western blots of the different fractions (same as before) were incubated with the panel of antibodies recognizing the respective members of the complex. S3 was used again as marker of the ribosomal fraction.

While in the presence of RNAguard MID1-FLAG associated with ribosomes (Figure 3.20A), after treatment with RNaseA, MID1-FLAG could not sediment with the ribosomal fraction anymore (Figure 3.20B). Surprisingly, in spite of the presence of a cocktail of protease inhibitors in the sample, MID1 also disappeared from the lysate. Given that it was present in the lysate before treatment , this suggests that MID1 is not stable without RNA. Probably it precipitated or was degraded by proteases that were not inhibited by the used cocktail (Complete mini, see methods section) and that only can access the protein when it is not bound to RNA. On the other hand, DNaseI treatment (Figure 3.20C) did not affect MID1 stability or ribosome association.

EF-1α and NPM, proteins of the complex closely related to ribosomes, showed a pattern similar to MID1-FLAG. Before RNaseA treatment they were present in the lysate, and after treatment, they disappeared and, consequently, were not found in the ribosomal pellet (Figure 3.20B). Other proteins like Hsc70 and ANXA2, while being present in the lysate after RNase treatment, they lost their association to the ribosomal pellet in the absence of RNA (Figure 3.20B). As expected, neither RNaseA nor DNaseI treatment affected the sedimentation properties of integral components of the ribosomes, such as RACK1 and S3 (Figure 3.20B, lanes 6,7).

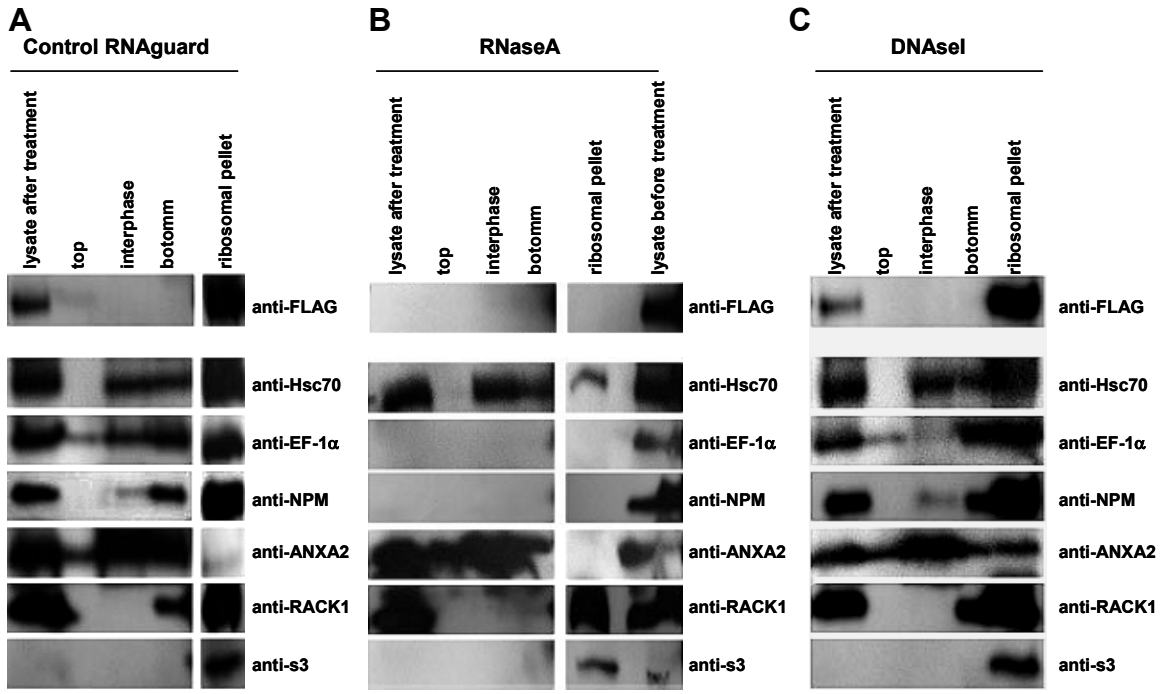

Figure 3.20. The MID1 complex requires RNA to associate with ribosomes
Discontinuos 20%-50% sucrose gradients were run with cytosolic HeLa cell extracts after RNA guard treatment (**A**) or treatment with RNase A (**B**) or DNAse I (**C**). The lysate and four different fractions, corresponding to the top of the gradient, the interphase (20% layer), the bottom (interface between 20% and 50%) and the ribosomal pellet, were tested on Western blots with the indicated antibodies. For the experiment treated with RnaseA, the lysate prior to treatment is also shown.

3.2.9 Characterisation of the association of MID1-FLAG with ribosomes

Having shown that the MID1 complex associates with ribosomes in an RNA-dependent manner, a battery of different conditions were tested to further characterise this association. Thus, discontinuous sucrose gradients were run, this time using a swing-out rotor in order to allow a more precise definition of the different phases.

3.2.9.1 Salt and detergent treatments

In order to analyse if the MID1 complex association to ribosomes is influenced by salt or detergent, cytoplasmic extracts of HeLa cells overexpressing MID1-FLAG were treated with 0.5 mM KCl or 0.5% deoxycholate (DOC). Same fractions were studied as previously described on Western blots developed with anti-FLAG antibody.

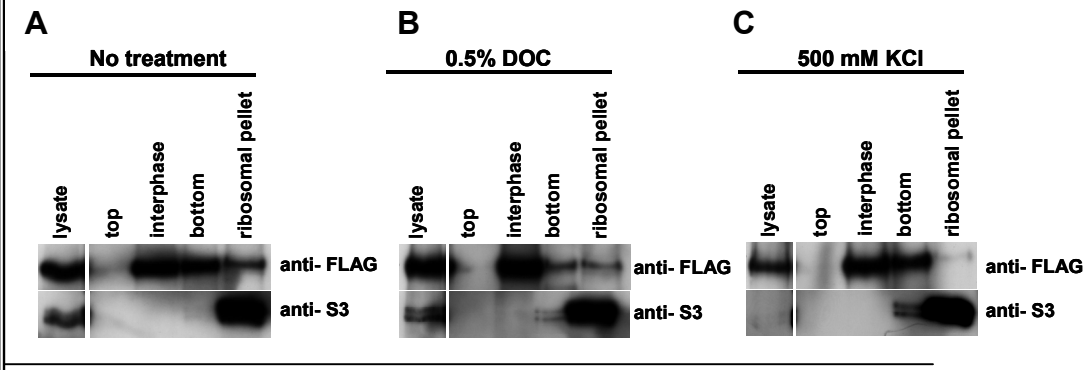

Figure 3.21. Characterisation of MID1 complex association with ribosomes
The lysate (left lanes) and four different fractions of a 20%-50% discontinous sucrose gradient were loaded (left lane). Top: upper part of the gradient containing the lysate; Interphase: 20% sucrose layer; Bottom: interface between 20% and 50%.
Results without treatment (**A**), with 0.5% DOC (**B**) and 500 mM KCl (**C**) are shown, from left to right. S3 is used to identify the ribosomal fraction.

Again, without treatment, MID1-FLAG sediments with S3 in the ribosomal pellet (Figure 3.21A). However, the better definition of the phases, due to a slower sedimentation process in the swing-out rotor, leads to a major retention of MID1-FLAG in the different fractions. After addition of 0.5% DOC (Figure 3.21B) or 500 mM KCl (Figure 3.21C) to the cytosolic extracts, most of MID-FLAG was washed off from the ribosomal pellet. Of note, KCl had stronger consequences than DOC.

3.2.9.2 EDTA treatment

For further characterisation, HeLa cell lysates were treated with EDTA, which destroys ribosome integrity, and compared to detergent treatment. In contrast to S3, which as an integral component of the small ribosomal subunit remained in the ribosomal pellet, EDTA presence lead to dissociation of MID1-FLAG from the ribosomes (Figure 3.22). This indicates that active ribosomes are necessary for association with MID1-FLAG.

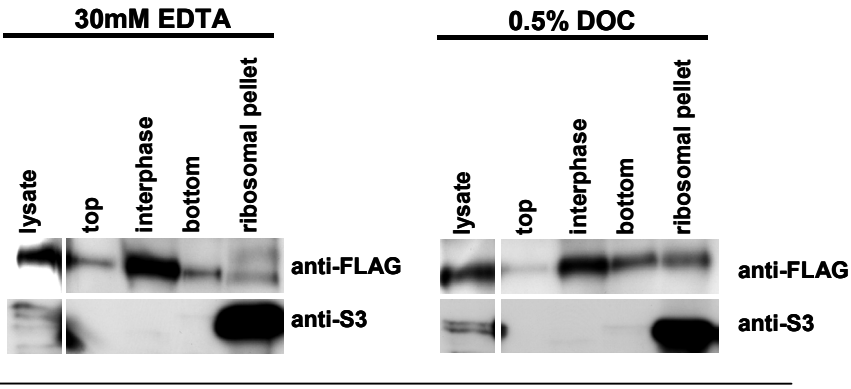

Figure 3.22. EDTA effect on ribosome association of the MID1 complex
The lysate (left lanes), and four different fractions of a 20%-50% discontinous sucrose gradient are shown. Top: upper part of the gradient containing the lysate; Interphase: 20% sucrose layer; Bottom: interface between 20% and 50%. Western blots were probed with anti-FLAG (upper lane) and anti-S3 (lower lane)
Effects of 30 mM EDTA are shown (left panel) compared to 0,5% DOC (right panel).

3.2.9.3 Puromycin and cycloheximide treatments

Finally, effects of puromycin compared to cycloheximide were likewise examined. While puromycin provokes the disassembly of the ribosomes from RNA leading to disruption of polyribosomes, cycloheximide stops translation by blocking polyribosome run-off. Same experiments as before were done but, in order to reduce complexity, only the interphase, the lysate and the ribosomal pellet were examined.

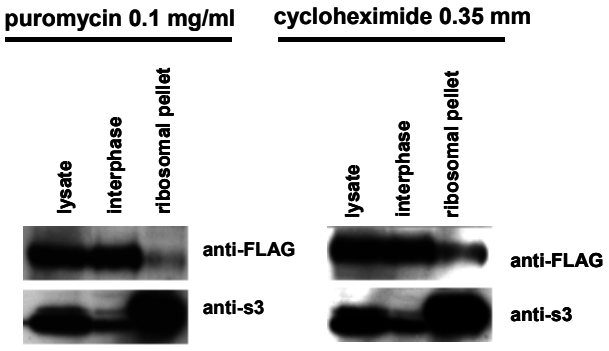

Figure 3.23. puromycin/cycloheximide
The lysate (left lane), the interphase and the ribosomal pellet fractions of a 20%-50% sucrose gradient are shown. Western blots were probed with anti-FLAG (upper lane) and anti-S3 (lower lane). Left panel shows the effects of puromycin- and right panel the effects of cycloheximide-treatment.

As predicted, cyclohexidime treatment preserved the association of MID1-FLAG with the ribosomal fraction (Figure 3.23). In contrast, puromycin caused dissociation, indicating that the MID1 complex associates with active polyribosomes and that their disruption leads to MID1 dissociation from the ribosomal fraction.

3.2.10. Endogenous MID1 and other components of the complex associate with ribosomes

Having established MID1-FLAG association with ribosomes, the endogenous situation was analysed and this time, additional members of the MID1 complex were included in the study. Same procedure as before with a swing-out rotor, and KCl and DOC treatments, was followed, but this time HeLa cell extracts did not contain MID1-FLAG.

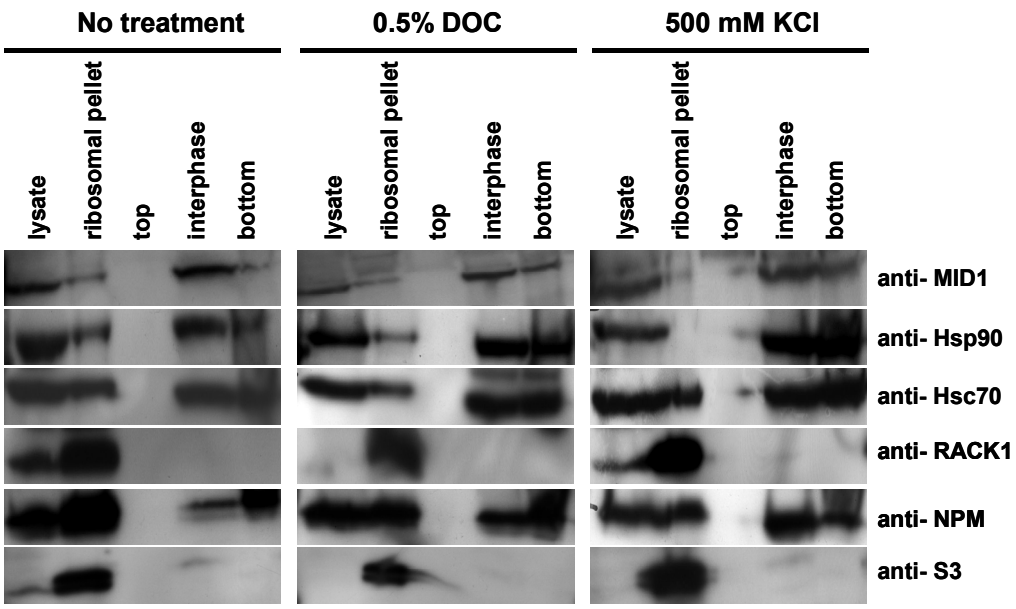

Figure 3.24. Endogenous situation

The lysate (left lane) and four different fractions of a 20%-50% discontinous sucrose gradient were loaded on a 10 % SDS-gel and probed on Western blots with different antibodies. Top: upper part of the gradient containing the lysate; Interphase: 20% sucrose layer; Bottom: interface between 20% and 50%.

The effects of adding 0.5% DOC or KCL are shown compared to the situation without treatment (right to left).

As shown in Figure 3.24, endogenous MID1 associates with ribosomes (tracked by the presence of S3) similar to overexpressed MID1-FLAG (Figure 3.24) and, accordingly, DOC and KCl (Figure 3.24, middle and right panels) washed off the protein from ribosomes, with KCl exhibiting a stronger influence. Interestingly, not all the complex components showed the same sedimentation properties in the gradient after salt and detergent treatment. While Hsp90 was washed off from the ribosomes with KCl, and partly with DOC, Hsc70 sedimentation properties were not affected under any of the experimental conditions tested. Some other members of the complex such as NPM and RACK1 are closely related to ribosomes and, as expected, their association with the ribosomal fraction was not affected with any of the treatments (Figure 3.24).

3.2.11 MID1 associates with polyribosomes

In section 3.2.9, it was shown that disruption of polyribosomes with puromycin or disassembly of ribosomal subunits with EDTA leads to dissociation of MID1 from the ribosomal fraction, suggesting that the MID1 complex associates not only with active ribosomes but also with active polyribosomes. To verify this, HeLa extracts were run through a continuous 15%-45% sucrose gradient in an SW40 swing-out rotor. Fractions were collected while measuring RNA absorbance at 254 nm, indicative of ribosomes or polyribosomes presence, precipitated, and analysed by Western blots incubated with anti-MID1 and with anti-S3, as a ribosomal marker.

The first peak of the chromatogram (Figure 3.25A) from the left corresponds to the top of the gradient, which contains the lightest ribosomal subunit, 40S. The next big peak corresponds to the entire ribosome, 80S. The big subunit, 60S, is found overlapping with 80S as a little deviation of the peak to the left. The last fractions of the gradient contain polyribosomes; at least eight peaks corresponding to different amounts of associated ribosomal monomers are observed.

S3 was again used as a ribosomal marker. Co-sedimentation of the two proteins, MID1 and S3 throughout in all fractions of the gradient could be observed (Figure 3.25), confirming that MID1 had gone through the entire gradient (Figure 3.25). Consequently, it could be demonstrated that the MID1 complex associates with active polyribosomes and forms a big ribonucleic protein complex (RNPs).

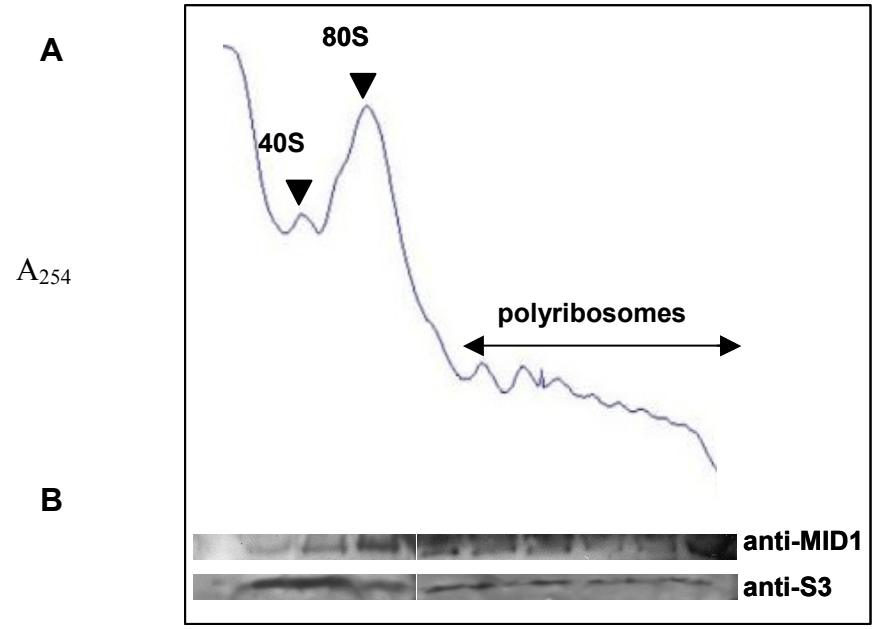

Figure 3.25. Sucrose gradient

A. Chromatogram showing absorbance of the sucrose gradient at 254 nm. Fractions containing 40S ribosomal subunits, 80S ribosomes and polyribosomes are indicated. **B**. Western blot of the different fractions developed with anti-MID1 antibody. Anti-S3 was used as ribosomal marker.

3.2.12 MID1 associates with homoribopolymers

Knowing that the MID1 complex associates with ribosomes in an RNA dependent manner (section 3.2.8) and that some members of the complex, such as ANXA2, bind directly to RNA (Filipenko et al., 2004), a possible direct interaction between the MID1 complex and RNA was studied.

A classic way to assay RNA binding properties of a protein is to test it for interaction with homoribopolymers. Some to date well-established RNA binding proteins like Fragile mental retardation protein (FMRP), ANXA2 or poly(A)-binding protein have been thereby characterised (Brown et al., 1998; Burd et al., 1991; Filipenko et al., 2004). Likewise, the MID1 protein complex was analysed for RNA binding properties. Following standard procedures, cytosolic HeLa cell extracts overexpressing MID1-FLAG were incubated with homoribopolymers - rU, rG, rA and rC. After extensive washing, bound proteins were boiled off and analysed on Western blots with a panel of antibodies detecting the respective proteins of the complex. Incubation of the membrane with anti-HuR antibody, a protein known to interact with U-rich stretches (Lopez de Silanes et al., 2004), was used as control to confirm the specificity of the reaction.

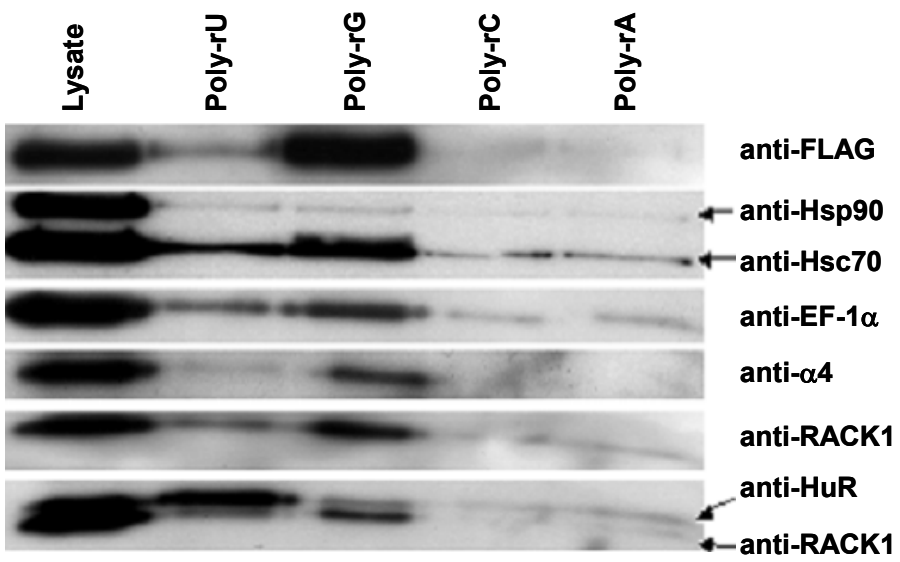

Figure 3.26. The MID1 complex associates with homoribopolymers
HeLa cell cytosolic extracts were incubated with poly-rU,-rG,-rC and –rA homoribopolymers. Western blots of the bound proteins incubated with the indicated antibodies are shown. HuR, a U-rich stretches binding protein, was used as control.

Specific bands corresponding to FLAG-MID1, Hsp90, Hsc70, EF-1α and RACK1 were detected in the rG-homopolymer- (Figure 3.26) and, although much weaker, in the rU-homopolymer sample. As expected, HuR showed a stronger binding to poly-rU homoribopolymers, confirming the specificity of the interaction.

3.2.13 Characterisation of the Poly-rG-MID1 binding

In order to characterise the interaction of the MID1 complex with poly-rG, a series of different experimental conditions was tested. Increasing amounts of NaCl and heparin were used to check the resistance of the interaction to ionic forces. Competition assays by increasing amounts of free poly-rG and free poly-rU were also performed.

Although much weaker compared to the non-treated control, MID1-FLAG could still associate to poly-rG in the presence of 250 mM NaCl and 1 mg/ml heparin (Figure 3.27A), increasing NaCl concentration up to 500 mM and heparin up to 2 mg/ml destroyed almost the entire interaction.

Competition experiments with free poly-rG and polyrU confirmed the specificity of the reaction between the MID1 complex and immobilized homopolymers. As shown in Figure 3.27B, addition of free poly-rG or free poly-rU 1:1 already produced a notable decrease of the interaction with agarose bound poly-rG. The addition of free homoribopolymers 1:10 led to almost total disruption of the association on the MID1 complex to bound poly-rG.

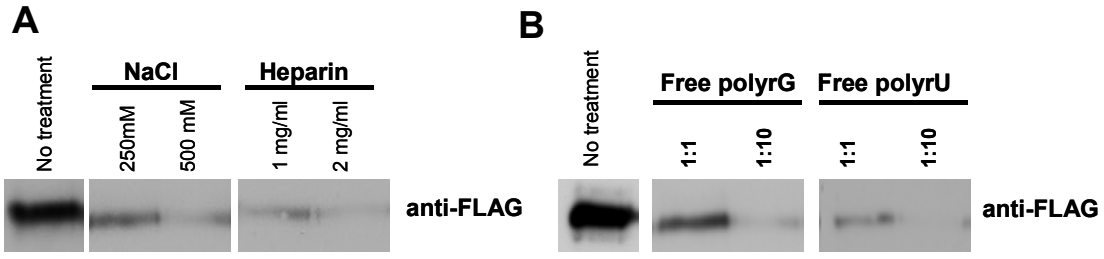

Figure 3.27. RNA binding properties of MID1

A. Influence of increasing concentrations of NaCl and heparin on the association of MID1 complex with poly-rG. **B**. Competition experiments with increasing amounts of free poly-rG. The ratio given is bound:free poly-rG. In both cases, bound proteins were boiled off and the presence of MID1-FLAG was confirmed on Western blots incubated with anti-FLAG antibody.

In order to test if the zinc-binding protein domains of MID1, RING and/or Bboxes, are involved in the association of the protein complex with RNA, cell extracts of HeLa cells overexpressing MID1-FLAG, FLAG-tagged constructs lacking Bbox1 or Bbox2 and GFP-tagged constructs with MID1 lacking either the RING-finger domain or the RING-finger and both Bboxes were incubated with poly-rG homoribopolymers. As described above, after extensive washing bound proteins were boiled off and analysed by Western blotting with anti-FLAG or anti-GFP antibodies.

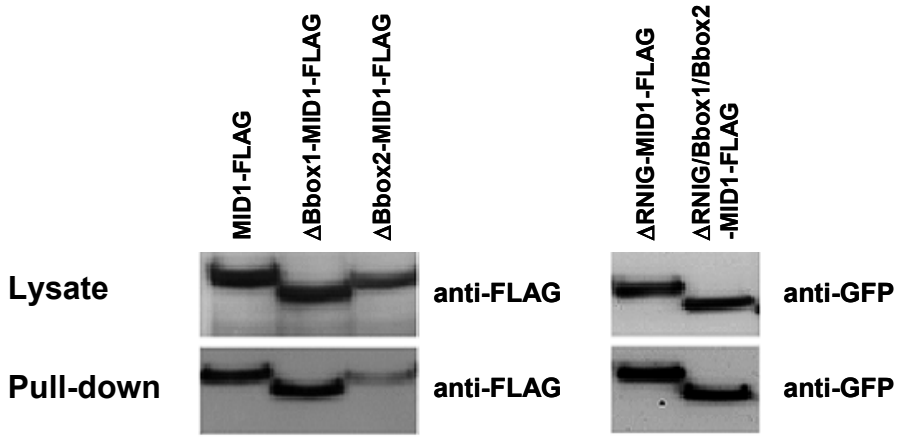

Figure 3.28. MID1 direct interaction with RNA

Pull-down experiments with poly-rG and HeLa cell extracts overexpressing different MID1 consruct. Western blots of lysates and poly-rG pull-downs were incubated with anti-FLAG or anti-GFP antibodies.

All mutant MID1 proteins associated with poly-rG stretches, (Figure 3.28), showing that neither the RING-finger nor the Bboxes are directly involved in the association of the MID1 complex with RNA.

3.2.14 MID1 complex binds ephrin mRNA via G-quartet structures

In order to get an idea of specific mRNAs that might be associated to the MID1 complex described, a candidate strategy applying phenotype and protein function comparisons was used. As outlined earlier, patients with craniofrontonasal dysplasia present with mutations in the ephrin-B1 gene (*EFNB1*), a member of the ephrin family of proteins (Twigg et al., 2004; Wieland et al., 2004). The phenotype of this patients highly resembles facial features of patients with OS. The remarkable phenotypic overlap of the two syndromes, plus a functional overlap of ephrins and MID1 during NCC migration, makes ephrins attractive candidates to be related to the MID1/α4 complex. Specifically, as the MID1/α4 complex might play a role in localising RNAs to distinct subcompartments of the cell, it is reasonable to consider the mRNAs of Eph receptor and ligand genes as potential targets of this complex. Given that the MID1 protein complex had been shown to bind poly-rG, EphB receptor and ephrin-B mRNAs were screened for the presence of G-quartets, which are G-rich motifs that were first described in mRNA targets of the fragile X mental retardation protein (FMRP) complex and that have been shown to be responsible for RNA localisation. Based on G-quartet sequences described in the literature (Brown et al., 2001; Darnell et al., 2001; Ramos et al., 2003) combined with re-analysis of known target genes of FMRP (Brown et al., 2001; Kaytor and Orr, 2001), a consensus sequence for the prediction of G-quartet structures was extracted (Figure 3.29A). Based on Bioperl regular expressions, an algorithm for the prediction of such mRNA structures was made in collaboration with the bioinformatics department at Max Planck Institute for Molecular Genetics (http://genereg.molgen.mpg.de/cgi-bin/regEchse/regEchse.pl). Following this algorithm, EphB receptor and ephrin-B mRNAs, as well as the 3´and 5´UTR of all genes available in the ENSEMBL database, were scanned for the presence of putative G-quartets.

A

```
[AT]GG\w{1,4}[AT]GG\w{1,4}[AT]GG\w{1,4}[AT]G
```

B

EFNB1	a-TGG{A} AGG{C} AGG{GC} TGG	at position 2071
	b-TGG{GGTA}AGG{GGC} AGG{CC} AGG	at position 2388
	c-TGG{GGGG}TGG{AGGG}AGG{TG} AGG	at position 2673
	d-TGG{GC} TGG{GGCC}TGG{AAAG}AGG	at position 2911
EFNB2	a-AGG{GAG} TGG{GGC} TGG{GGAA}AGG	at position 1745
	b-TGG{GAA} AGG{AAC} AGG{CT} TGG	at position 2005
EPHB1	a-AGG{GAAA}AGG{ACC} AGG{GTCA}AGG	at position 3203
EPHB2	a-AGG{G} TGG{GAAG}AGG{TGAG}TGG	at position 140
	b-TGG{TCAC}AGG{G} TGG{TTT} TGG	at position 3806
EFNB3	a-TGG{G} TGG{GAAG}AGG{TGAG}TGG	at position 616
	b-AGG{TCC} TGG{C} AGG{GTC} AGG	at position 3745
	c-AGG{GC} AGG{C} AGG{GGC} AGG	at position 3986
EFNB4	a-TGG{GTG} TGG{TCC} TGG{TCC} TGG	at position 1724
EFNB6	a-AGG{G} TGG{CTGT}TGG{AGGA}AGG	at position 5
	b-AGG{AGC} AGG{G} TGG{TGGC}TGG	at position 137

Figure 3.29. G-quartets in ephrin genes

A. Consensus sequence for the prediction of G-quartets **B**. G-quartet motifs identified in five Eph receptor and two ephrin mRNAs

In two ephrins, six G-quartet like structures were identified, EFNB1a-d and EFNB2a, b (Figure 3.29B). To note, in *EFNB1*, the gene mutated in patients with craniofrontonasal dysplasia, four G-quartet like structures were spotted. Moreover, nine different G-quartet like structures were found in five different Eph receptors, EPBH1, EPBH2a,b, EPBH3a-c, EPBH4 and EPHB6a,b (Figure 3.29B). Interestingly, while one or more G-quartets were found in either the 5´or 3´ UTR in 22% of all genes from the ENSEMBL database, only 1,33% of the analysed genes contained more than three G-quartets (Table2).

Number of G-quartet motifs	1	2	3	>3	Total found
3' UTR	3053	1128	443	357	4981
5' UTR	1342	235	66	51	1694
Total number of genes searched : 30686					6675

Table 3.2. G-quartet predictions

Number of 3' or 5' UTRs containing varying numbers (1, 2, 3 or >3) of G-quartet structures from a set of 30686 genes available in ENSEMBL.

3.2.15 Binding of the G-quartets to the MID1 Complex

Subsequent to identification of G-quartet like structures in the ephrin genes, it was tested whether these structures indeed associate with the MID1 complex. Some of the identified G-quartet motifs were PCR amplified with primers including the T7 promotor sequence at the 5´ end. Primer sequences were chosen such that approximately fifty base pairs were flanking both ends of the G-quartet in order to allow proper folding of the structure. Obtained PCR products were purified and *in vitro* transcribed in the presence of biotinylated-UTP. Subsequently, the transcripts were incubated with cytosolic extracts of HeLa cells overexpressing MID1-FLAG. Biotin transcripts were pulled down with streptavidin coated magnetic beads, and extensively washed. Bound proteins were finally boiled off and checked on Western blots that were probed with anti-FLAG antibody (Figure 3.30).

All four G-quartets of EFNB1 (EFNB1a-d), EFNB2a and motifs of several Eph receptors (EPBH6a, b, EPBH3c, EPBH2b and EPBH1) were tested for MID1 complex interaction (Figure 3.30). While most of them were confirmed to associate with MID1-FLAG (Figure 3.30), two of them, EPBH4 and EPBH6a, did not show association with MID1-FLAG. The specificity of the reaction could be further confirmed by controls done with the antisense sequence of one of the motifs, EFNB1b, or with a sample that did not contain RNA.

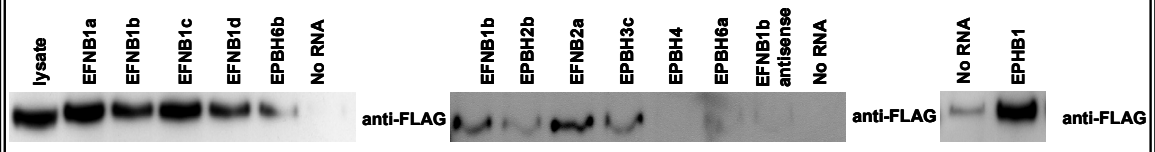

Figure 3.30. MID1 association with G-quartet structures in ephrin genes
PCR amplified, in-vitro transcribed and biotinylated G-quartet sequences were incubated with MID1-FLAG overexpressing HeLa cells lysates. Bound proteins were boiled off and the presence of MID1-FLAG was confirmed on Western blots incubated with anti-FLAG antibody. The indicated G-quartets were used in this study

Posterior incubation of the blots with different antibodies allowed the study of other member of the complex. Thus, incubation with anti-EF-1α, anti-NPM, anti-S3 and anti-RACK1 showed association of all of them to the G-quartets tested (Figure 3.31). Hsp90, a weaker interaction partner of the complex, and ANXA2, the RNA association of which has been described to be Ca^{2+} dependent, showed only background binding. Lysates were loaded to confirm the presence of all proteins.

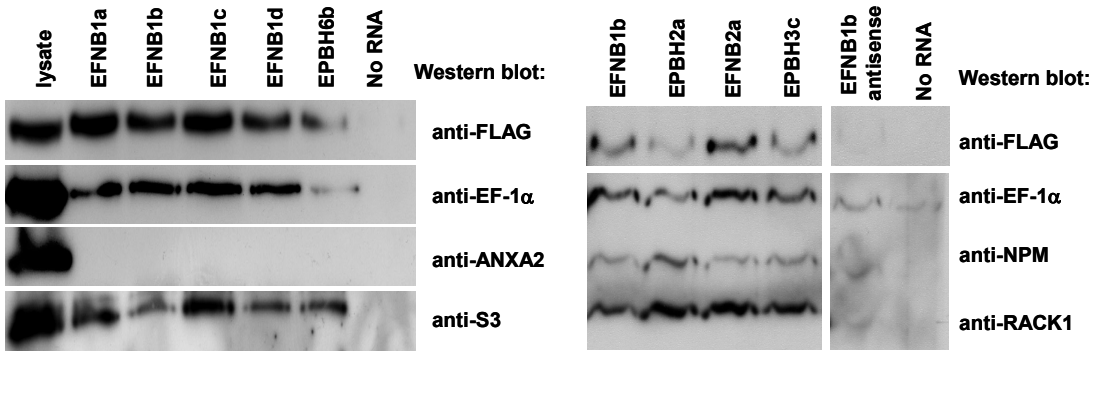

Figure 3.31. Association of components of the MID1 complex with G-quartets
The presence of different members of the complex in the elution fractions from the previous experiment was tested using the antibodies indicated.

One of the motifs, EFNB1b, was further characterised by studying the effect of salt on the interaction of G-quartets with MID1-FLAG. Same experiment as before was done but in the solution increasing amounts of salt were added (100-500 mM). A Western blot of the bound proteins probed with anti-FLAG antibody shows decrease in the EFNB1b-MID1 association with increasing amounts of salt, probing the specificity of the interaction (Figure 3.32).

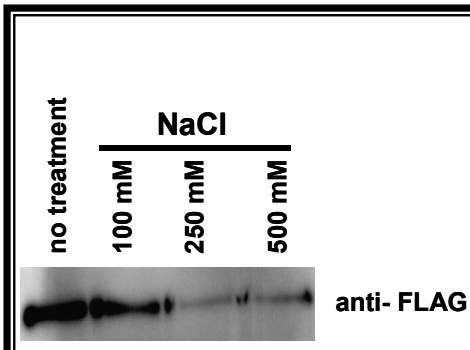

Figure 3.32. Influence of salt in EFNB1b-MID1 interaction.
HeLa cytosolic cell lysates with increasing amounts of NaCl were incubated with biotinylated-EFNB1b and pulled down with streptavidin coated beads. Bound proteins were analysed by Western blot with an anti-FLAG antibody and compared to an untreated control.

3.2.16 MID1 complex associates with EFNB1 *mRNA*

Finally, it was studied whether the MID1 complex associates with the entire mRNA of EFNB1, including the G-quartet containing 3´UTR. In addition, biotinylated transcripts containing none, one (+1Gq), two (+2Gq), three (+3Gq) or all four G-quartets (+4Gq) (Figure 3.33A) were analysed. Two antisense transcripts containing three (+3GqAS) and four (antisense) G-quartets (+4GqAS) and a sample without RNA were used as negative control.

Biotinylated transcripts were incubated with extracts of HeLa cells overexpressing MID1-FLAG and subsequently pulled down with streptavidin-coated beads. After washing, bound

proteins were boiled off, and the presence of MID1-FLAG was tested by Western blot analysis with anti-FLAG antibody. As shown in Figure 3.33B, MID1-FLAG associated with G-quartet containing transcripts in an additive manner; that is, the probe having a single G-quartet present almost no association to MID1, and the binding increased with increasing numbers of G-quartets. Maximal binding was obtained in the sample with four G-quartets. As expected, the probe without the 3´UTR did not bind to the MID1 complex, similarly to the sample without RNA. None of the antisense transcripts, which corresponded to the longest probes, showed any binding to the MID1 complex. This demonstrated that the reason for the additive effect is not the increasing length of the transcripts but the specific association of the MID1 complex to G-quartets.

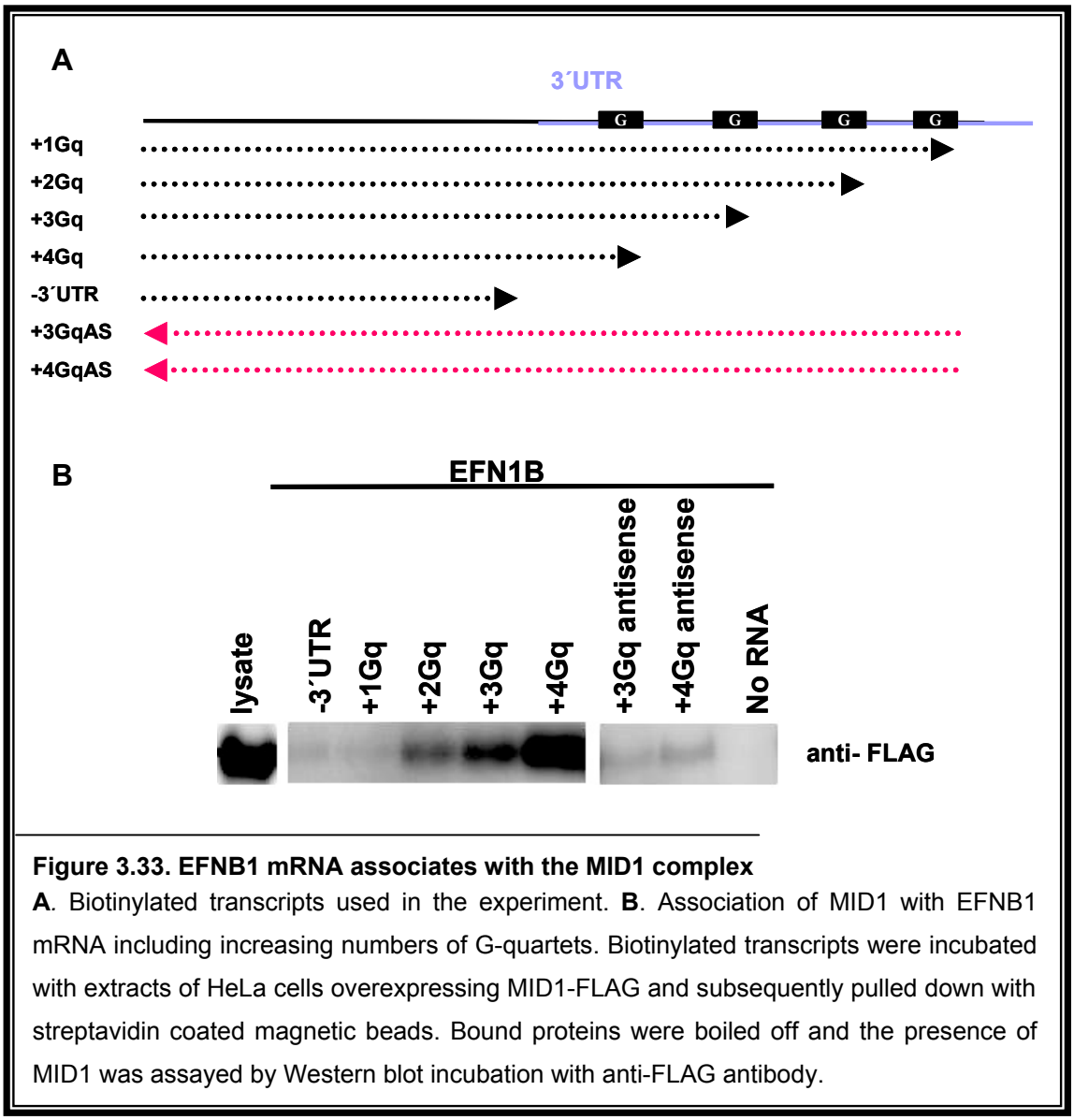

Figure 3.33. EFNB1 mRNA associates with the MID1 complex
A. Biotinylated transcripts used in the experiment. **B**. Association of MID1 with EFNB1 mRNA including increasing numbers of G-quartets. Biotinylated transcripts were incubated with extracts of HeLa cells overexpressing MID1-FLAG and subsequently pulled down with streptavidin coated magnetic beads. Bound proteins were boiled off and the presence of MID1 was assayed by Western blot incubation with anti-FLAG antibody.